Journal of the American College of Cardiology
© 2012 by the American College of Cardiology Foundation
Published by Elsevier Inc.

Vol. 60, No. 2, 2012
ISSN 0735-1097/$36.00
http://dx.doi.org/10.1016/j.jacc.2012.02.052

Multifocal Ectopic Purkinje-Related Premature Contractions

A New *SCN5A*-Related Cardiac Channelopathy

Gabriel Laurent, MD, PHD,* Samuel Saal, MD,† Mohamed Yassine Amarouch, PHD,‡§‖ Delphine M. Béziau, MSC,‡§‖ Roos F. J. Marsman, MSC,¶ Laurence Faivre, MD, PHD,† Julien Barc, PHD,‡‖ Christian Dina, PHD,‡‖ Geraldine Bertaux, MD,* Olivier Barthez, MD,* Christel Thauvin-Robinet, MD, PHD,† Philippe Charron, MD, PHD,# Véronique Fressart, MD, PHD,** Alice Maltret, MD,†† Elisabeth Villain, MD,†† Estelle Baron, BA,‡‖ Jean Mérot, PHD,‡§‖ Rodolphe Turpault, PHD,‡‡‖ Yves Coudière, PHD,‡‡‖ Flavien Charpentier, PHD,‡§‖§§ Jean-Jacques Schott, PHD,‡‖§§ Gildas Loussouarn, PHD,‡§‖ Arthur A. M. Wilde, MD, PHD,¶ Jean-Eric Wolf, MD, PHD,* Isabelle Baró, PHD,‡§‖ Florence Kyndt, PHARMD, PHD,‡‖‖‖ Vincent Probst, MD, PHD‡‖§§

Dijon, Nantes, and Paris, France; and Amsterdam, the Netherlands

Objectives The aim of this study was to describe a new familial cardiac phenotype and to elucidate the electrophysiological mechanism responsible for the disease.

Background Mutations in several genes encoding ion channels, especially *SCN5A*, have emerged as the basis for a variety of inherited cardiac arrhythmias.

Methods Three unrelated families comprising 21 individuals affected by multifocal ectopic Purkinje-related premature contractions (MEPPC) characterized by narrow junctional and rare sinus beats competing with numerous premature ventricular contractions with right and/or left bundle branch block patterns were identified.

Results Dilated cardiomyopathy was identified in 6 patients, atrial arrhythmias were detected in 9 patients, and sudden death was reported in 5 individuals. Invasive electrophysiological studies demonstrated that premature ventricular complexes originated from the Purkinje tissue. Hydroquinidine treatment dramatically decreased the number of premature ventricular complexes. It normalized the contractile function in 2 patients. All the affected subjects carried the c.665G>A transition in the *SCN5A* gene. Patch-clamp studies of resulting p.Arg222Gln (R222Q) Nav1.5 revealed a net gain of function of the sodium channel, leading, in silico, to incomplete repolarization in Purkinje cells responsible for premature ventricular action potentials. In vitro and in silico studies recapitulated the normalization of the ventricular action potentials in the presence of quinidine.

Conclusions A new *SCN5A*-related cardiac syndrome, MEPPC, was identified. The *SCN5A* mutation leads to a gain of function of the sodium channel responsible for hyperexcitability of the fascicular-Purkinje system. The MEPPC syndrome is responsive to hydroquinidine. (J Am Coll Cardiol 2012;60:144–56) © 2012 by the American College of Cardiology Foundation

From the *CHU Dijon, Service de Cardiologie, Hôpital le Bocage, Dijon, France; †CHU Dijon, Centre de Génétique, Hôpital d'Enfants, Dijon, France; ‡INSERM, UMR1087, l'institut du thorax, Nantes, France; §CNRS, UMR6291, Nantes, France; ‖Université de Nantes, Nantes, France; ¶Department of Experimental Cardiology, Heart Failure Research Center, Academic Medical Center, Amsterdam, the Netherlands; #AP-HP, GH Pitié Salpêtrière, Département de Cardiologie, and UPMC Univ Paris 6, Département de Génétique, INSERM UMR-S956, Paris, France; **AP-HP, GH Pitié Salpêtrière, UF Cardiogénétique et Myogénétique Moléculaire et Cellulaire, Service de Biochimie Métabolique et Centre de Génétique, Paris, France; ††Cardiologie Pédiatrique, Université Paris V René Descartes, Hôpital Necker-Enfants Malades, Paris, France; ‡‡CNRS, UMR6629, Laboratoire de Mathématiques Jean Leray, Nantes, France; §§CHU Nantes, l'institut du thorax, France; and the ‖‖CHU Nantes, Service de génétique médicale, Nantes, France. Dr. Amarouch is currently at the University of Bern, Department of Clinical Research, Bern, Switzerland. Dr. Barc is currently at the University of Amsterdam, Department of Experimental Cardiology, Academic Medical Center, Amsterdam, the Netherlands. The Agence Nationale de la Recherche financially supported Drs. Turlpault and Coudière (ANR-07-JCJC-0141), Dr. Baró (ANR-09-GENO-003-01), and Dr. Schott (ANR-05-MRAR-028-01). Dr. Schott was also supported by a Leducq Foundation Trans-Atlantic Network of Excellence grant (05 CVD 01). The research leading to these results has also received funding from the European Community's Seventh Framework Programme FP7/2007–2013 under grant agreement

Primary arrhythmogenic disorders of the heart are a major cause of sudden cardiac death in otherwise healthy individuals with structurally normal hearts. Mutations in several genes encoding ion channels and channel-interacting proteins have emerged over the last decade as the basis for a variety of inherited cardiac arrhythmias (1–3). Different mutations in a single gene may account for various disorders depending on the position of the mutation, the nature of the amino acid substituted, the type of the mutation (non-sense, false-sense. . .), and its functional consequences (4,5).

The *SCN5A* gene encodes the pore-forming subunit of the voltage-gated Na^+ channel Nav1.5. In the heart, this channel plays a key role in rapid impulse propagation through the conduction system and in the excitability of atrial and ventricular cardiomyocytes. Mutations in *SCN5A* are responsible for a spectrum of hereditary arrhythmias, including type-3 long QT (LQT3) syndrome, the Brugada syndrome, cardiac conduction disease, sinus node dysfunction, atrial fibrillation, and dilated cardiomyopathy (see Tfelt-Hansen et al. [6] for a review) (5,7–13). In addition to these syndromes, originally regarded as independent entities, recent evidence shows considerable clinical overlap, implying new disease entities known as overlap syndromes of the cardiac Na^+ channel (14).

In this article, we report a novel autosomal dominant form of cardiac arrhythmia identified in 3 unrelated families and characterized by multifocal ectopic Purkinje-related premature contractions (MEPPC). This arrhythmia is due to the c.665G>A *SCN5A* mutation leading to a shift in p.Arg222Gln (R222Q) Nav1.5 voltage dependency.

Methods

An expanded Methods section is available in the Online Appendix.

Clinical evaluation. This study was in agreement with the local guidelines for genetic research and has been approved by the local ethical committees. Informed, written consent was obtained from each family member who agreed to participate to the study. Standard 12-lead electrocardiography, Holter recording, and echocardiography were proposed to all participating family members. We also proposed electrophysiological studies to some patients.

Patients were considered affected when ventricular arrhythmia corresponding to MEPPC was detected.

Mutation analysis. Genomic DNA was extracted from peripheral blood lymphocytes using standard protocols. The proband (III.1) of Family 1 was screened for mutations in known genes responsible for dilated cardiomyopathy (DCM) and arrhythmia, including *LMNA* encoding lamin A/*C*, *ABCC9* encoding SUR2A, and *SCN5A* (10,15,16).

Haplotype analysis. Ten microsatellite markers around the *SCN5A* gene (D3S1759, D3S2432, D3S3047, D3S3512, D3S1298, intragenic *SCN5A* marker, D3S3521, D3S3527, D3S3522, and D3S3559) were genotyped. We estimated the age of the mutation using the Genin et al.'s method (17).

Cellularelectrophysiology. Patch-clamp studies were performed on COS-7 cells transiently expressing human wild-type (WT) or R222Q Nav1.5 (NG_008934) and human β1 subunits, using the whole-cell configuration at room temperature (18).

Mathematical modeling. Single-cell models of the human Purkinje cells (19) and left ventricular myocytes (20) were used. Both models were incorporated in a multicellular model and the propagation of the electrical waves in the cardiac tissues was described by a monodomain model (21). The numerical simulations were performed on a simplified 2D slice model described previously (22).

Statistics. All data are presented as mean ± SEM. The statistical significance of the observed effects was assessed by the Student *t* test or 2-way analysis of variance (ANOVA) followed by a Tukey test for multiple comparisons when needed. A p value <0.05 was considered significant.

Abbreviations and Acronyms

- **AF** = atrial fibrillation
- **ANOVA** = analysis of variance
- **AP** = action potential
- **DCM** = dilated cardiomyopathy
- **ECG** = electrocardiogram
- **ICD** = implantable cardioverter-defibrillator
- **LBBB** = left bundle branch block
- **LQT** = long QT syndrome
- **LVDd** = left ventricular diastolic diameter
- **LVEF** = left ventricular ejection fraction
- **MEPPC** = multifocal ectopic Purkinje-related premature contractions
- **NSVT** = nonsustained ventricular tachyarrhythmia
- **PAC** = premature atrial complex
- **PVC** = premature ventricular complex
- **RBBB** = right bundle branch block
- **TTE** = transthoracic echocardiogram
- **VT** = ventricular tachycardia

Results

We identified 3 families affected by the same phenotype, segregating with an autosomal dominant pattern over 3 generations (Fig. 1A). In Family 1, 11 of 18 family members were affected, 4 of 5 members were affected in Family 2, and 6 of 8 members were affected in Family 3. Patient characteristics are summarized in Tables 1 and 2.

Clinical results. CLINICAL PHENOTYPE OF THE FAMILY 1 PROBAND (PATIENT III.1). Patient III.1 was identified at the age of 10 years after mild dyspnea while exercising. Her 12-lead surface electrocardiogram (ECG) showed a chaotic

n°FP7-HEALTH-2009-single-stage 241526 (Drs. Baró and Charpentier). Dr. Loussouarn was financially supported by the Association Française contre les Myopathies (n° 14120) and Dr. Charpentier by the Fondation pour la Recherche Médicale (DVC20070409253). All other authors have reported that they have no relationships relevant to the contents of this paper to disclose. Drs. Laurent, Saal, and Amarouch contributed equally to this work. Drs. Baró, Kyndt, and Probst contributed equally to this work as senior authors.

Manuscript received October 13, 2011; revised manuscript received January 19, 2012, accepted February 14, 2012.

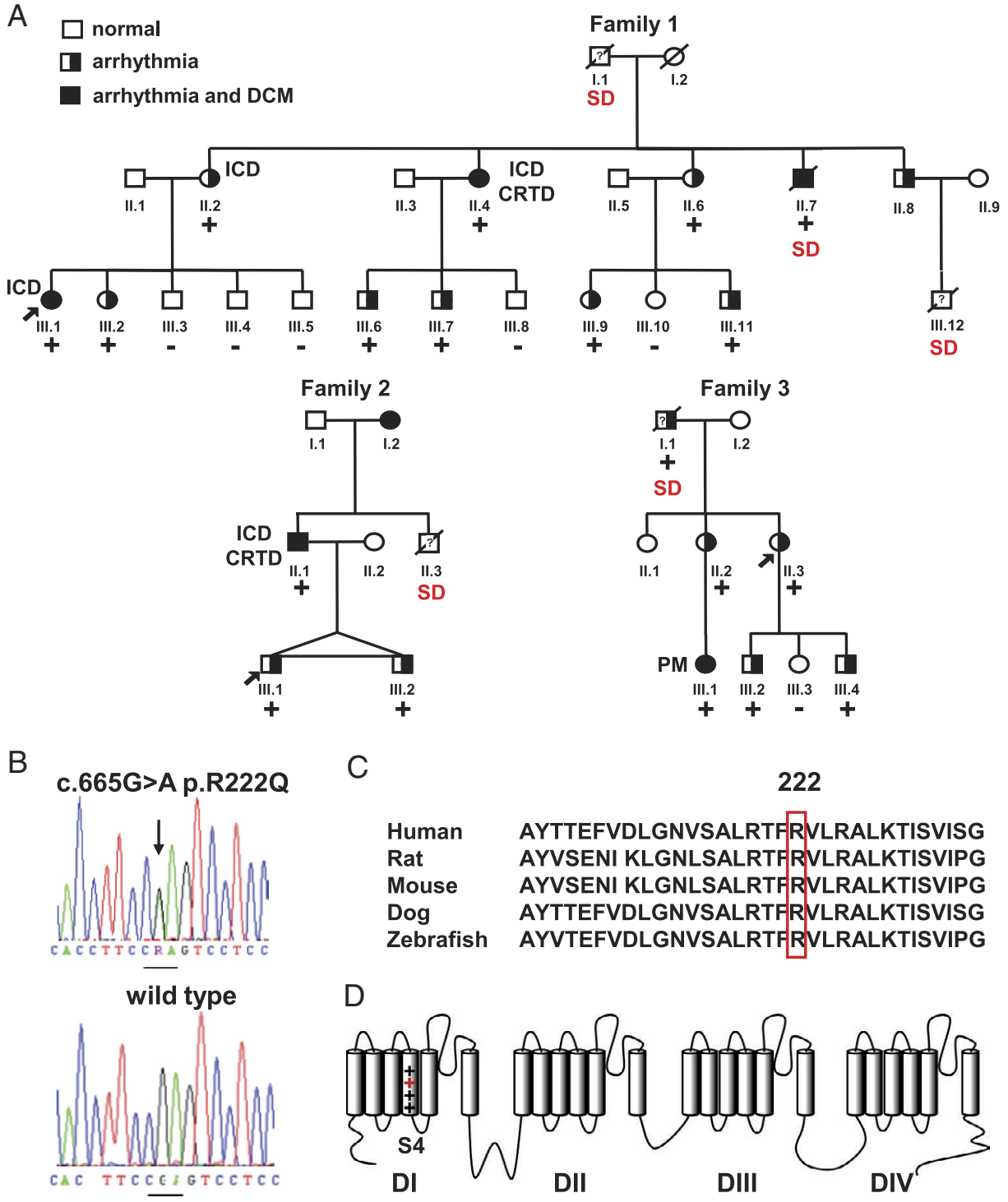

Figure 1 ***SCN5A* Mutation**

(A) Pedigree and phenotype of the 3 families. Members affected with arrhythmia are indicated with a **half-filled symbol**. Members affected with arrhythmia and dilated cardiomyopathy (DCM) are indicated in **black**. **Question marks** indicate undetermined phenotype. Males and females are indicated by **squares** and **circles**, respectively. Probands are indicated by **arrows**. **Diagonal lines** indicate the deceased individuals. Individuals carrying the mutation are indicated **(+)**. Individuals who tested negative for the mutation are indicated **(-)**. An implantable cardioverter-defibrillator (ICD) was implanted in 4 patients, 2 of whom also had a cardiac resynchronization therapy defibrillator (CRTD) and 1 of whom had a DDD pacemaker (PM). Sudden death (SD) was reported in 5 individuals. **(B)** Mutation analysis of *SCN5A* revealed a heterozygous c.665G>A missense mutation in affected individual III.1 that results in a p.Arg222Gln (p.R222Q) amino acid substitution. **(C)** Multiple alignment analysis shows conservation of the Arg222 (R222) amino acid among species. **(D)** Structure of Nav1.5. The p.Arg222Gln mutation is located in the voltage-sensing S4 segment of domain I (DI).

Table 1 Clinical Data of the Family Members

Patient #	Age at Diagnosis (yrs)	Mean Follow-Up (yrs)	QTc (ms)*	Gender	Symptoms	LVDd (mm/m^2)	LVEF Before Medication (%)	Atrial Arrhythmia	PVC Morpho†	PVC Axis	Junction Rhythm	NSVT‡	Total PVC/ 24 h	EPS	PVC Regression at Exercise
Family 1															
I.1	29	—	—	M	SD	—	—	—	—	—	—	—	—	No	—
II.2	29	17	423	F	Syncope	55	73	Paroxysmal atrial arrhythmia	R	R and L	Yes	No	62,000	No	Yes
II.4	37	8	358	F	Dyspnea	61	35	No	R and L	R and L	Yes	Yes	>25,000	Yes	Yes
II.6	25	20	426	F	Dyspnea	48	59	No	—	R and L	No	No	—	No	—
II.7	23	27	362	M	Dyspnea, SD	60	47	No	—	R and L	Yes	No	—	No	—
II.8	17	19	391	M	Syncope	55	60	No	—	—	No	No	—	No	—
III.1	10	7	361	F	Syncope	40	32	Paroxysmal atrial arrhythmia	R and L	R and L	Yes	Yes	>50,000	Yes	Yes
III.2	0§	5	365	F	No	33	60	No	—	—	Yes	No	—	No	—
III.6	12	9	380	M	Palpitations	51	47	No	R and L	R and L	Yes	Yes	>25,000	Yes	Yes
III.7	17	5	360	M	Dyspnea	46	67	No	R and L	R and L	Yes	No	>25,000	No	Yes
III.9	25	3	407	F	No	—	—	No	no	no	Yes	No	200	No	—
III.11	15	3	413	M	No	—	—	No	no	no	Yes	No	11	No	—
III.12	4 months	—	—	M	SD	—	—	No	—	—	—	—	—	No	—
Family 2															
I.2	—	—	—	F	—	—	—	—	—	—	—	—	—	No	—
II.1	35	8	410	M	Palpitations	—	—	No	—	no	No	—	—	Yes	—
II.3	11	0	420	M	SD	—	—	Atrial flutter	—	—	—	—	—	No	—
III.1	6	7	405	M	No	36	60	No	L	R and L	Yes	No	18,000	No	Yes
III.2	12	0.5	408	M	Presyncope	33	60	No	L	R and L	Yes	No	86,000	Yes	Yes
Family 3															
I.1	62	9	—	M	SD	—	—	Atrial bigeminy	R and L	—	Yes	Yes	—	—	—
II.2	29	26	414	F	Palpitations	28	58	Paroxysmal atrial arrhythmia	R and L	R and L	Yes	Yes	60,000	No	Yes
II.3	18	36	431	F	Palpitations	28	>50	Atrial fibrillation	R and L	R and L	Yes	Yes	7,134	Yes	Yes
III.1	7	12	399	F	Dyspnea	36	35	Paroxysmal atrial arrhythmia	R and L	R and L	Yes	Yes	35,650	No	Yes
III.2	14	6	415	M	Near collapse	31	>50	Atrial flutter	R and L	L	Yes	No	17,706	Yes	Yes
III.4	14	2	430	M	Palpitations	29	>50	Paroxysmal atrial arrhythmia	—	—	Yes	Yes	3,516	No	—

*Bazett-corrected QT interval (QTc) measured on lead II of most recent electrocardiogram under sinus rhythm. †Premature ventricular contractions (PVCs) with right (R) and left (L) bundle branch block patterns. ‡Nonsustained ventricular tachyarrhythmia (<30 s). §Gestation of 24 weeks.

EPS = electrophysiological study; LVDd = left ventricular diastolic diameter; LVEF = left ventricular ejection fraction; SD = sudden death.

Table 2 Follow-Up and Treatment of the Family Members

Patient #	Treatment	ICD	CRTD	Symptoms on Treatment	PVC/24 h on Medication	LVEF on (Before) Medication (%)	Sudden Death	*SCN5A* Mutation
Family 1								
I.1	—	No	No	—	—	—	Yes	—
II.2	Hydroquinidine	Yes	No	No	<5,000	60 (73)	No	Yes
II.4	Hydroquinidine	Yes	Yes	No	<5,000	50 (35)	No	Yes
II.6	Amiodarone	No	No	Yes	4	—	No	Yes
II.7	None	No	No	—	—	—	Yes	Yes
II.8	None	No	No	—	—	—	No	—
III.1	Hydroquinidine	Yes	No	No	<5,000	56 (32)	No	Yes
III.2	None	No	No	—	—	—	No	Yes
III.6	*	No	No	Yes	—	—	No	Yes
III.7	None	No	No	—	—	—	No	Yes
III.9	None	No	No	—	—	—	No	Yes
III.11	None	No	No	—	—	—	No	Yes
III.12	—	No	No	—	—	—	Yes	—
Family 2								
I.2	None	No	No	—	—	—	No	—
II.1	Amiodarone	Yes	Yes	Yes	—	45 (20)	No	Yes
II.3	—	No	No	—	—	—	Yes (11)	—
III.1	Hydroquinidine	No	No	No	2,500	60 (60)	No	Yes
III.2	Hydroquinidine	No	No	No	7,700	60 (60)	No	Yes
Family 3								
I.1	—	—	—	—	—	—	Yes (71)	Yes
II.2	Flecainide	No	—	No	125	58	No	Yes
II.3	Flecainide	No	—	No	5,791	>50 (>50)	No	Yes
III.1	PropafeNon†	DDD PM	—	Yes	31,894	50 (35)	No	Yes
III.2	Flecainide	No	—	Yes	486	52 (>50)	No	Yes
III.4	Flecainide	No	—	No	21	>50 (>50)	No	Yes

*Flecainide, nadolol, sotalol, or verapamil. Hydroquinidine treatment and ICD implantation were proposed but refused by the patient. †Patient III.1 started on flecainide as well, however, she did not tolerate this drug. The patient is currently treated with propafenon, on subtherapeutic doses.

CRTD = cardiac resynchronization therapy defibrillator; DDD PM = DDD pacemaker; ICD = implantable cardioverter-defibrillator; LVEF = left ventricular ejection fraction; PVC = premature ventricular contractions.

cardiac rhythm comprising narrow junctional and rare sinus beats competing with premature ventricular complexes (PVCs) showing various right bundle branch block (RBBB) patterns (Fig. 2A). There was an overdrive suppression of the PVCs during treadmill exercising. Signal-averaged ECG did not show late potentials. A Holter monitoring device recorded more than 50,000 PVCs per 24 h. The transthoracic echocardiogram (TTE) revealed a mild dilation of the left ventricle (left ventricular diastolic diameter [LVDd] 54 mm or 40 mm/m^2, above 97th percentile) (23), but a normal left ventricular ejection fraction (LVEF) (62%). She remained asymptomatic until the age of 13 years, when she was referred for brief sudden loss of consciousness at rest. The ECG exhibited recurrent nonsustained ventricular tachyarrhythmias (NSVTs) with RBBB patterns, which were concomitant with several fainting episodes (Fig. 2B). Several nonsustained supraventricular arrhythmias have been identified during the follow-up. New TTE showed a markedly enlarged LVDd (62 mm), and a decreased LVEF (32%). A dual-chamber implantable cardioverter-defibrillator (ICD) was then implanted associated with oral hydroquinidine treatment. Once the measured plasma level of the drug reached 1 mg/l (normal range 1 to 3 mg/l), this medication succeeded in markedly reducing the number of PVCs (Table 2). After 1 year under hydroquinidine treatment, the PVC burden was <1% and her heart was considered normal in TTE (LVDd 54 mm, LVEF 56%).

Clinical investigation of family members allowed the identification of 10 other affected individuals with similar ECG characteristics (Online Fig. 1).

CLINICAL PHENOTYPE OF THE FAMILY 2 PROBAND (PATIENT III.1) AND HIS TWIN BROTHER (PATIENT III.2). Patient III.1 was identified at age 6 years because of an irregular heart rate without any other symptoms. His twin brother was diagnosed at 12 years with the same arrhythmia after experiencing syncope while cycling. A complete clinical evaluation including a TTE and magnetic resonance imaging was normal, but his ECG showed frequent PVCs with a left bundle branch block (LBBB) pattern, and superior and inferior axial deviation (Fig. 2C). In both patients, the Holter ECG recorded tens of thousands of PVCs per 24 h (Table 1). Exercise allowed a clear decrease of their number. Both patients were finally treated with hydroquinidine, leading to a dramatic decrease of the PVC number (Table 2).

A patient III.1 family 1 at 10 years old

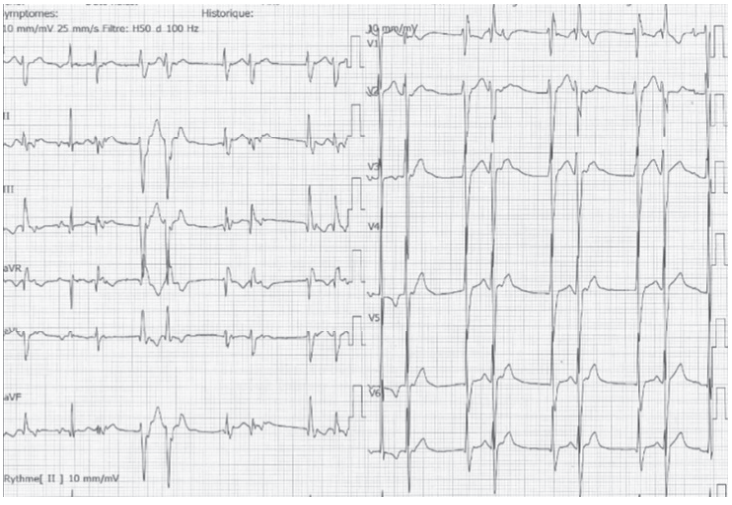

B patient III.1 family 1 at 13 years old

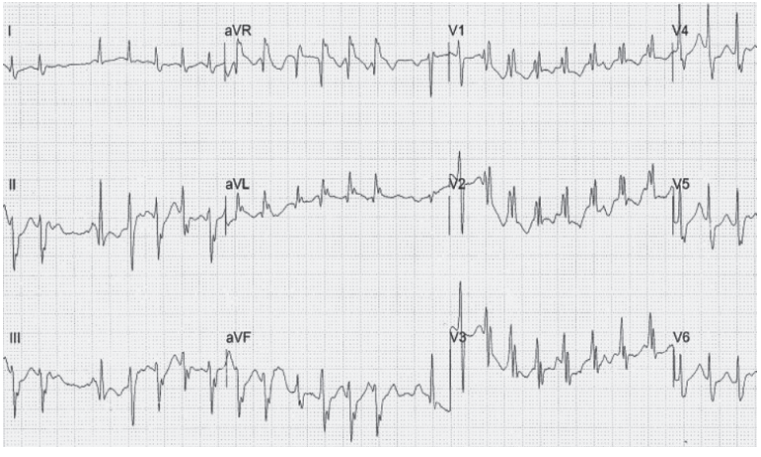

C patient III.1 family 2

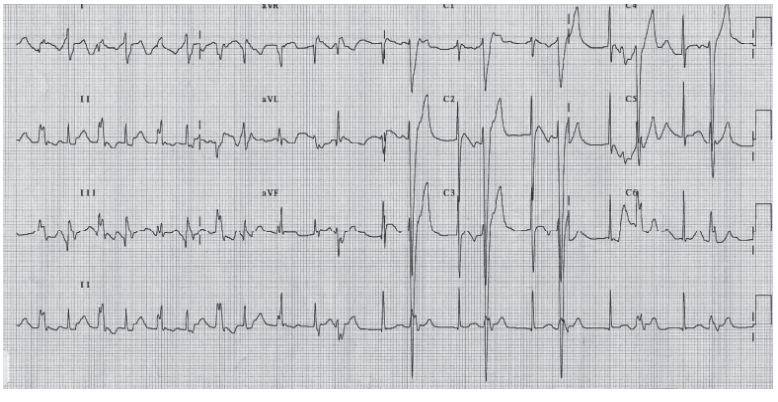

Figure 2 **Representative ECG Tracings of the Families**

(A) Representative 12-lead surface electrocardiogram (ECG) of Family 1, 10-year-old proband (Patient III.1), showing a chaotic cardiac rhythm including normal sinus and junctional QRS complexes competing with various right bundle branch block pattern complexes corresponding to PVCs. **(B)** Symptomatic nonsustained ventricular tachyarrhythmia recorded on the same patient as in **(A)**, at 13 years old (right bundle branch block pattern, QRS axis variation). QRS morphologies are changing from one beat to another. **(C)** Twelve-lead surface ECG of Patient III.1 of Family 2 showing a chaotic cardiac rhythm with rare sinus beats and alternant junctional rhythms with ventricular bigeminisms. Premature ventricular complexes had left bundle branch block pattern with slight variations in shape and axis.

Their father and grandmother had both been affected with DCM associated with frequent PVCs, and 1 uncle, known as affected by atrial flutter, had died suddenly at age 11 years.

CLINICAL PHENOTYPE OF THE FAMILY 3 PROBAND (PATIENT II.3). The index patient II.3 was identified at the age of 18 years during a routine medical examination. Her 12-lead ECG showed premature atrial complexes (PACs), atrial fibrillation (AF), pre-excitation on the ECG, and frequent relatively narrow PVCs with both LBBB and RBBB patterns. Electrophysiological testing revealed ectopic foci from the atria, the atrioventricular junction, and the bundle branches. The accessory pathway was located at the right septal site. At the age of 48 years, Holter monitoring recorded a permanent chaotic supraventricular rhythm with >48,900 PACs and >7,000 isolated and bigeminal PVCs (35% and 5% of total QRS complexes, respectively). Flecainide therapy marginally reduced ventricular ectopies; however, it completely suppressed supraventricular arrhythmia (Holter monitoring recorded <150 PACs, representing <1% of total QRS complexes). Flecainide therapy was maintained because hydroquinidine is not available in the Netherlands, where Family 3 lives.

A REMARKABLY CONSTANT PHENOTYPE. Within these 3 families, 21 individuals were affected by PVCs. Patient characteristics are summarized in Tables 1 and 2. Despite the various ages at diagnosis, from 24 weeks of gestation to 62 years (mean age 20 years; n = 20), the phenotype was remarkably constant: narrow sinus and junctional QRS complexes (n = 17) competing with various complexes showing an RBBB or LBBB patterns (n = 15), corresponding to PVCs with superior or inferior axes. We did not observe any QT prolongation (Table 1) or ST-segment elevation.

PVCs were isolated, or paired (bigeminism) with sinus or junctional QRS complexes. NSVTs were identified in 8 individuals. Five patients were affected by syncope or presyncope. Sudden death was reported in one 4-month-old boy (Patient III.12 in Family 1), an 11-year-old boy (Patient II.3 in Family 2), and 3 adult males (29, 50, and 71 years old; Patients II.7 and I.1 in Family 1 and Patient I.1 in Family 3). However, PVCs were clearly identified in only 2 of these cases (Patient II.7 in Family 1 and Patient I.1 in Family 3) before sudden death. Episodes of syncope or fainting during polymorphic ventricular tachycardia (VT) episodes (Holter or ICD monitorings) were reported in 3 females (Fig. 2B). Two individuals in Family 1, 1 in Family 2, and 6 in Family 3 presented with atrial arrhythmia (PACs, nonsustained atrial tachyarrhythmia, or AF). One patient had AV conduction disturbances. Only 1 patient in Family 3 had an accessory pathway.

ELECTROPHYSIOLOGICAL STUDY. Electrophysiological testing was performed in 7 cases (Fig. 3, Online Fig. 2). Pre-systolic potentials recorded at ectopic sites during PVCs either corresponded to Purkinje potentials during normal sinus beats or to the proximal extension of the left anterior and posterior fascicles (Figs. 3B and 3C). In all tested patients, numerous ectopic foci were identified along the left conduction system and its proximal extension. We did not record any PVCs from the myocardium itself as the local ventricular electrograms were always preceded by a Purkinje potential and we did not record any retrograde Purkinje potential activation or slow conduction area in the Purkinje network. Reentrant mechanisms were excluded because no PVCs or VTs could be pacing induced and no mid diastolic potentials were recorded during VT (24–26).

When tried on Patient II.4 of Family 1, radiofrequency applications did not eradicate PVCs as the whole Purkinje tissue was involved in triggering PVCs from varying sites. Whereas we proposed electrophysiological studies to most of the patients, not all of them accepted. Among affected members in the 3 families, PVC features were very similar with a sharp slope of the first ventricular deflection and close characteristics to authentic LBBB or RBBB patterns with right or left axis. In patients who underwent an electrophysiological study, we identified those PVC morphologies as being triggered from Purkinje fibers. We therefore inferred that similar PVC patterns may originate from similar Purkinje regions in the other patients.

EVOLUTION OF THE LEFT VENTRICULAR FUNCTION ON ANTI-ARRHYTHMIC TREATMENT. Transthoracic echocardiograms were performed in all affected patients and magnetic resonance imaging was performed in 3 cases. Low LVEF with dilation of the left ventricle was identified in 7 patients. Several antiarrhythmic treatments were attempted within the families (Table 2). Amiodarone treatment was partially successful in 2 cases (Patient II.6 in Family 1 and Patient II.1 in Family 2). For patient II.1 in Family 2, amiodarone and cardiac resynchronization therapy defibrillator treatment were introduced simultaneously, partially normalizing the LVEF (from 20% to 45%). Hydroquinidine was successful in 5 cases with a dramatic decrease in the number of PVCs per 24 h (Table 2), and dramatically decreased the PVC number and improved the ventricular function in all cases. Patient III.1 was the first person to be treated by hydroquinidine in Family 1 and no adverse effects were noticed after 4 years of follow-up. Flecainide therapy was used in 5 patients and greatly reduced supraventricular and ventricular arrhythmias, with a clear decline in ventricular tachycardia episodes, in 3 of them. Other antiarrhythmic drugs were used in 4 patients but were successful in 3 cases only (Table 2).

An ICD was implanted in 4 patients, 2 of which had a cardiac resynchronization therapy defibrillator. Only 1 patient (Family 3) had atrioventricular conduction disturbances and was implanted with a double chamber pacemaker (Table 2).

Genetic results. MUTATION ANALYSIS. Because the first proband identified (Family 1, Patient III.1) had DCM, mutations in *LMNA* encoding lamin A/*C* and *ABCC9* encoding SUR2A, genes reported to be associated with DCM, were searched in this patient although unsuccess-

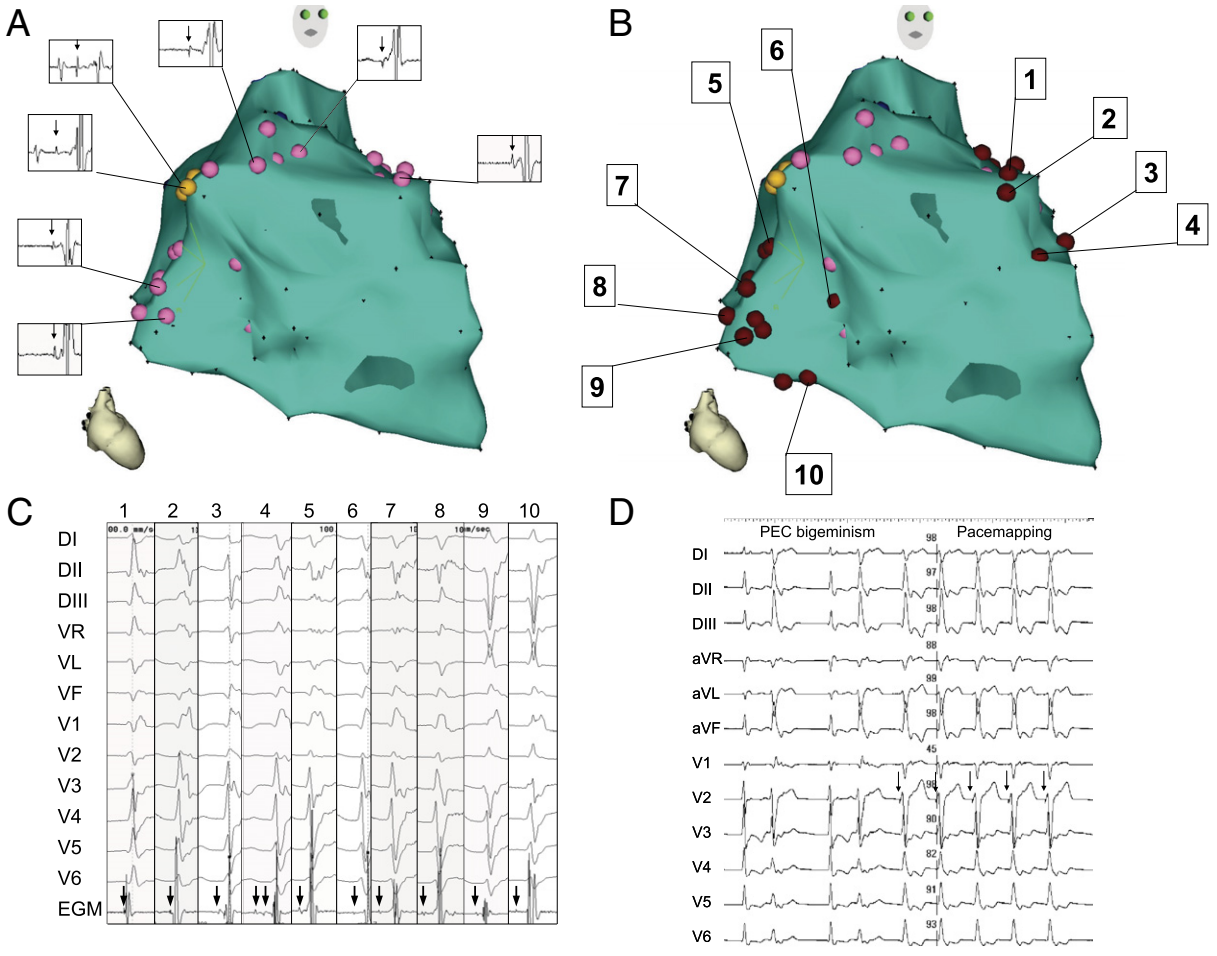

Figure 3 **Endocardial Electroanatomic Mapping of the Left Ventricle**

(A) Mapping of the left ventricle during sinus rhythm (Patient II.4, Family 1). Identification of the left specific conduction system. **Pink** and **yellow** tags present with a short sharp, high frequency, and low amplitude potential preceding the ventricular electrograms (EGMs) **(arrows)**. Note that the area with yellow tags represents the His bundle region, and those with pink tags represent the left anterior and posterior fascicles. **(B and C)** Mapping of the left ventricle during 10 different Purkinje-related ectopic contractions (same patient as in **A**). Identification of the different ectopic foci along the left specific conduction system. Pink and yellow tags as in **A**. **Red** tags indicate sites with single short sharp, high frequency, and low amplitude potentials preceding the premature ventricular complexes (PVC) EGMs. Sites are labeled from 1 to 10 according to corresponding 12-lead PVC morphologies (recording at 100 mm/s). Ectopic sites during PVCs were identified along the Purkinje network **(A)** or the proximal extension of the left anterior and posterior fascicles. The arrows denote the Purkinje potentials. **(D)** Pace mapping from the same patient as in **A**. **Right** shows 12-lead surface ECG (25 mm/s) during PVC bigeminism. **Left** shows pacing at the earliest local activation during PVCs (local presystolic potential) reproduced a very close match to the surface ECG (except for V_1). Numbers are percentages of pacing concordance for each lead (from 45% at V_1 to 99%, mean 90%).

fully. The *SCN5A* gene, reported to be associated with DCM and various arrhythmogenic diseases, was also sequenced. Genetic testing of Family 1's proband revealed that she was heterozygous for a c.665G>A transition in *SCN5A* exon 6 (Fig. 1B), resulting in the substitution of an arginine for a glutamine at position 222 (R222Q). This substitution is located in the voltage-sensing S4 segment of domain I of the cardiac Na^+ channel Nav1.5 (Fig. 1D). Subsequently, the mutation was detected in Family 2's (Patient III.1) and Family 3's (Patient II.3) probands who did not present DCM. The mutation was 100% penetrant and strictly segregated with the cardiac arrhythmia in all the families, consistent with a mutation-related disease (Fig. 1A). It was absent in 600 control chromosomes. The Arg222 (R222) amino acid is highly conserved across species (Fig. 1C). This mutation is reported on dbSNP (rs45546039) but at 0% in all populations and is not reported in the National Heart, Lung, and Blood Institute Exome variant server.

HAPLOTYPE ANALYSIS. To investigate whether a common ancestral chromosome accounted for the recurrence of the R222Q mutation in unrelated Families 1, 2, and 3, we constructed mutation-associated haplotypes by genotyping family members for 10 microsatellite markers (Online Fig. 3, Online Appendix: Results).

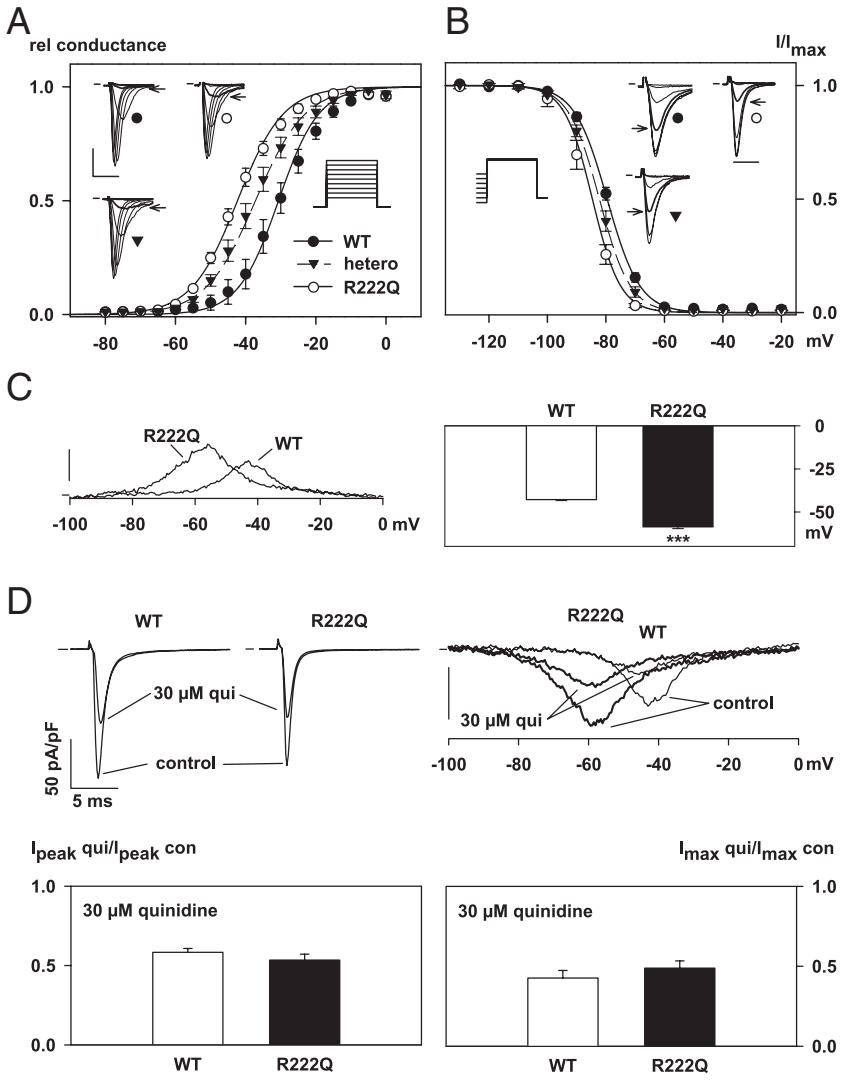

Figure 4 **Experimental Effects of R222Q Mutation on Nav1.5 Channel in COS-7 Cells**

(A) Relative peak conductance versus membrane potential curves for Nav1.5 channels in COS-7 cells transfected with wild-type (WT), R222Q Nav1.5 or both, in the presence of WT β1 subunit. **Curves** are Boltzmann fits to the data show the mutation-dependent activation shift. **Inset** shows stimulation protocol and superimposed Na^+ current recordings during 20-ms depolarizations to various potentials from −80 to +0 mV (holding potential –100 mV; 10-mV increment; frequency 0.5 Hz). **Scale bars** are 2 ms, 1,000 pA. **Bold trace** and **arrow** are Na^+ current at –50 mV. **(B)** Steady-state channel availability curves for Nav1.5 channels. Data are mean normalized peak current (I/I_{max}) measured at –20 mV versus pre-pulse voltage. **Curves** show Boltzmann fits to the data. **Inset** shows stimulation protocol and superimposed Na^+ current recordings at –20 mV after 500-ms polarization to various potentials from –110 to –50 mV (holding potential –100 mV; 10-mV increment; frequency 0.25 Hz) in COS-7 cells transfected as in **A**. **Scale bar** is 2 ms. **Bold trace** and **arrow** show Na^+ current at −80 mV. **(C)** Mean WT (n = 13) and R222Q (n = 14) tetrodotoxin-sensitive window currents (30 μM TTX) obtained with a depolarizing-voltage ramp (0.5 mV/ms, frequency 0.5 Hz), normalized to the peak current at –20 mV (I_{peak}) recorded in the same cell (**scale bar** 1% I_{peak}), and mean voltage at which the measured conductance was maximal (n = 12 and 14 for WT and R222Q, respectively). ***$p < 0.001$. **(D)** Effects of quinidine on WT and R222Q Nav1.5 currents. **(Left)** Representative WT and R222Q Na^+ currents recordings during 20-ms depolarizations to –20 mV (holding potential –100 mV; frequency 0.5 Hz) in the absence (control) and presence of 30 μM quinidine (qui), and mean residual current ratio (I_{peak} qui/I_{peak} con) in each condition (**bottom**; n = 12 and 10 for WT and R222Q, respectively). **(Right)** Mean window tetrodotoxin-sensitive current density (30 μM TTX), in the absence and presence of 30 μM quinidine, of WT **(thin line)** and R222Q **(bold line)** channels and mean residual current ratio (I_{max} qui/I_{max} con) measured when the conductance was maximal, in each condition (at −43 mV, n = 6; and at –59 mV, n = 7, for WT and R222Q, respectively). **Scale bar** is 2 pA/pF, same voltage protocol as in **C**.

Our data demonstrate that a founder effect for the R222Q mutation in these 3 families is very unlikely.

EFFECTS OF R222Q MUTATION ON NAV1.5 CHANNEL FUNCTION IN COS-7 CELLS. To investigate the functional consequences of the R222Q mutation on the Na^+ channel activity, we used the whole-cell configuration of the patch-clamp technique (Online Appendix: Results). The presence of the mutation did not modify the Na^+ current density (Figs. 4A and 4B, Online Table 1). The activation curve was shifted toward more negative potentials in the presence of the mutation (Fig. 4A, Online Table 1). Activation kinetics were accelerated in the mutant (Online Fig. 4A)

(2-way ANOVA, $p < 0.001$ vs. WT). Inactivation voltage sensitivity was also changed (Fig. 4B, Online Table 1), which, combined with the activation curve shift, predicted an increase of the window current availability (Online Fig. 5A). The maximum conductance of the tetrodotoxin-sensitive window current elicited by depolarizing-voltage ramps was not significantly different in R222Q Nav1.5 expressing cells, but the voltage at which the maximum conductance was measured was significantly shifted toward more negative values and the window current availability was increased when expressed as the area under the current-voltage curve (*t* test $p < 0.001$ and $p < 0.01$, respectively) (Online Table 1, Fig. 4C). Each of these changes caused a gain of function of the mutant channel. However, inactivation onset kinetics were also accelerated, causing a loss of function (Online Fig. 4B) (2-way ANOVA $p < 0.001$ vs. WT). Finally, kinetics of recovery from inactivation were not significantly modified by the R222Q mutation (Online Fig. 4C).

In order to understand the effects of hydroquinidine treatment on PVCs occurrence, we evaluated the WT and R222Q Na^+ current sensitivity to quinidine, its active form. At a concentration at which the WT peak I_{Na} was about half-reduced (30 μM in our conditions) (Online Table 2, Fig. 4D), WT and R222Q peak currents were similarly inhibited (2-way ANOVA $p < 0.001$ vs. control). When quinidine was tested on the window current, the inhibition was also similar in both groups when measured at the maximum conductance potential of each group (Fig. 4D, Online Table 2) (2-way ANOVA $p < 0.001$ vs. control). Therefore, WT and R222Q Na^+ currents were equally sensitive to quinidine.

A MULTICELLULAR COMPUTER MODEL TO CHARACTERIZE THE MOLECULAR AND CELLULAR EVENTS LEADING TO PREMATURE VENTRICULAR CONTRACTIONS. Because of the multiple and opposite effects of the mutation on channel activation and inactivation, its net effect on the action potential (AP) is not straightforward. To get insights on this effect, we carried out computer simulations and evaluated the impact of the mutation on AP in single-cell models of human Purkinje fibers and ventricles. Single-cell models of Purkinje and ventricular cell AP were run in WT and heterozygous conditions. In heterozygous conditions, incomplete repolarization occurred in Purkinje cell AP, correlated with an increased late Na^+ current (Online Fig. 6). The ventricular AP was much less affected (Online Fig. 6).

To evaluate the possibility of a causal role of the mutation on the generation of PVCs, we built a multicellular model incorporating both human cell models. In the WT condition, 1-Hz stimulation of the Purkinje fibers generated AP that propagated to the ventricle (Fig. 5Ba, Online Video 1A). Interestingly, in the heterozygous condition, incomplete repolarization in the Purkinje fibers triggered premature APs, propagating into the ventricles (Fig. 5Bb, Online Video 1B). Consistent with the disappearance of clinically observed PVCs during exercise, the triggered ventricular APs disappeared at higher pacing frequencies (2 Hz) (Fig. 2B, Online Video 2B). Altogether, these results: 1) strongly suggest that the gain of function of the Na^+ current predominantly affects the Purkinje cells; 2) explain the fact that the entire Purkinje system was affected resulting in a wide variety of ectopic foci; and 3) explain the frequency dependency of the PVCs.

Finally, the effects of quinidine were tested on the multicellular model. Clinically relevant effects of this drug are thought to be due to alteration of the Na^+ current, the transient outward current I_{to} (27,28), and the repolarizing delayed rectifier current I_{Kr} (29,30). In addition, quinidine also inhibits Ca^{2+} and other K^+ currents, although in a lower extent (31,32). Therefore, inhibition of these latter currents was not considered. In the model, the K^+ currents were reduced in parallel with the heterozygous Na^+ current. For the first test, we chose 10 μM quinidine, the maximal therapeutic dose (i.e., preserving 50% I_{Na}, 30% I_{Kr} [33], and 30% I_{to} [28]). In this case, we observed a normalization of the Purkinje and ventricular AP course at 1 Hz (not shown). To evaluate the effects of a more "therapeutic" dose of quinidine, we ran the model with lower current inhibition levels. As illustrated for the ventricular AP in Figure 5B, the normalization was still observed when the computed quinidine dose was reduced to preserve 75% I_{Na} and 45% I_{Kr} and I_{to}. However, when the computed quinidine dose was further reduced to preserve 85% I_{Na} and 50% I_{Kr} and I_{to}, triggered APs reappeared. Qualitatively, if not quantitatively, the multicellular model mimics the cardiac response to hydroquinidine treatment.

Discussion

We report a novel autosomal dominant form of cardiac arrhythmia showing MEPPC. MEPPC syndrome is characterized by frequent PVCs originating from various ectopic foci along the fascicular-Purkinje system occasionally associated with NSVTs and sudden death. Some patients (n = 9) also presented with PACs, nonsustained atrial tachyarrhythmias, or paroxysmal AF. In some patients, arrhythmias were associated with mild DCM. Hydroquinidine markedly reduced the number of PVCs and normalized the left ventricular function in patients with DCM. We demonstrate that a fully penetrant *SCN5A* gain-of-function mutation is responsible for this new syndrome.

Specificity of MEPPC. Ventricular arrhythmias originating from left ventricular fascicles have been described previously in patients with or without structural heart disease (ischemic or idiopathic cardiomyopathies) (24,25,34,35). Accounting for up to 30% to 50% of arrhythmias in nonischemic DCM, bundle branch re-entrant VTs usually have an LBBB pattern and enlarged QRS complexes with a prolonged H-to-V interval during sinus rhythm (34). Such conduction abnormalities were not identified in any of our patients.

Fascicular VT is the most common form of idiopathic left ventricular tachycardia occurring more frequently in young males without structural heart disease and with a particular sensitivity to verapamil (24). The ECG characteristics of

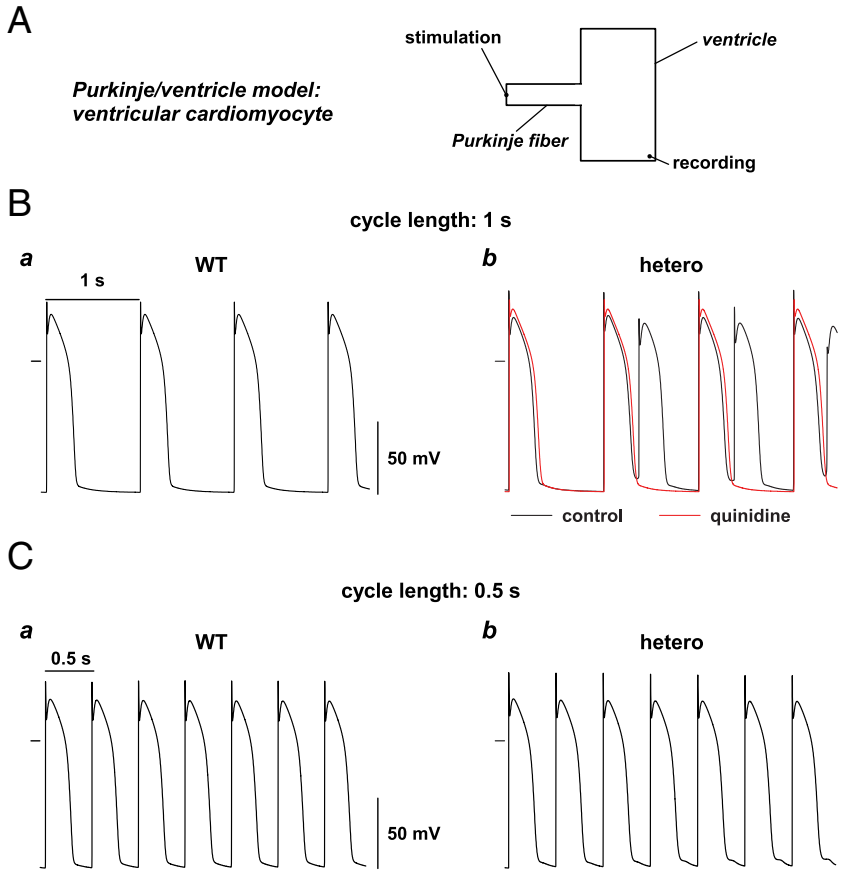

Figure 5 **Effects of the R222Q Mutation on a Ventricular Cardiomyocyte AP Obtained in the Purkinje/Ventricle Model**

(A) Dimensions of the calculation domain: Purkinje system 5 × 17.5 mm; ventricle 35 × 17.5 mm. Stimulation and recording sites are indicated. **(B and C)** Simulated action potential in a distal part of the ventricle in wild-type (WT) **(a)** and heterozygous **(b)** conditions with stimulation of a Purkinje cell at cycle length of 1 s **(B)** and 0.5 s **(C)**; and in the presence of quinidine (**Bb**; i.e., remaining 75% heterozygous I_{Na}, 45% WT I_{to} and 45% WT I_{Kr}; **red**) at 1 Hz. Also see Online Videos 1A, 1B, 2A, and 2B.

our patients were different. MEPPC syndrome was distinguished from PVCs originating from the posterior papillary muscle in the left ventricle (36) mainly by the presence of high-frequency potentials preceding local myocardial activation suggesting that Purkinje system was involved. Idiopathic VTs and bundle branch VTs typically present a single ECG morphology originating either near the posterior or the anterior left fascicle. In our patients, ECG characteristics demonstrated the varying origins of the PVCs, in either the left or right ventricle. Electrophysiological testing using a 3D endocardial navigation system clearly demonstrated that the PVCs originated from more than 10 different foci along the extension of the left anterior and posterior fascicles. This phenomenon was responsible for important changes in PVCs morphology (shape and axis) from one beat to another. Similar to triggered activities, the firing was fairly increased by isoproterenol infusion despite the increase in sinus rhythm at a lesser extent. As opposed to idiopathic fascicular VTs, which are well known to be highly sensitive to verapamil, this treatment had no effect on the tested affected family members. Atrial arrhythmias were less frequently observed than PVCs.

R222Q mutation causes the syndrome in 3 unrelated families. Several findings support the causative role of the R222Q *SCN5A* mutation in the pathogenesis of the disease in the 3 reported families: 1) the complete cosegregation of the mutation with the disease phenotype; 2) the identification of the same mutation in 3 unrelated families with a remarkably uniform phenotype; 3) the absence of the mutation in 300 ethnically matched control individuals; and 4) the high conservation of the R222 residue across species (Fig. 1C).

R222Q has been reported in a single patient with a Brugada syndrome (37). With the help of Dr. Xavier Waintraub (Hôpital Pitié-Salpêtrière, Paris, France) and the kind permission of Dr. Pascale Guicheney (INSERM UMR S956, Paris, France), we had the opportunity to re-evaluate the phenotype of this patient. He was clearly not affected by the Brugada syndrome, his ECG presenting no ST-segment elevation in the precordial leads. His phenotype appeared to be very closed to that of MEPPC syn-

drome with permanent junctional activity, very frequent multifocal ventricular premature beats (57,000 thin ventricular premature beats per day coming from left anterior and posterior fascicles), atrial arrhythmias, and dilated cardiomyopathy with moderated alteration of the ventricular contraction (LVEF 56%) (X. Waintraub, personal communication, September 2011). His familial history found that his mother and grandmother were also affected by DCM associated with frequent PVCs. None of the ECGs performed in patients harboring the *SCN5A* R222Q mutation met the ST-segment criteria for a Brugada syndrome.

The same *SCN5A* mutation was also detected in a cohort of 2,500 unrelated cases referred for LQTS genetic testing (38). However, none of the patients from the 3 families here presented a prolonged QTc. This may be explained by the relatively less impaired biophysical properties of the R222Q channel, mostly a negative shift of the window current, when compared with that of already reported LQT3-related mutants (5,39).

R222Q effects that we report on channel parameters were similar to those measured by Cheng et al. (40). In addition, we show that these effects are intermediate in the heterozygous state and that they also impair the window current, crucial during the AP plateau phase.

Looking for a mechanistic link between the genotype and the phenotype, we simulated the effect of the mutated channel activity on the Purkinje and ventricular electrical activity. Two points suggest that the shift in Nav1.5 voltage dependency is responsible for the premature ventricular contractions originating from the fascicular-Purkinje system. First of all, 1 of the particularities of this arrhythmia is that ectopic foci were observed in erratic locations of the Purkinje system, which made radiofrequency applications ineffective. The multicellular model shows that the impaired function of the Na^+ channels, anywhere in the Purkinje system, is sufficient enough to trigger premature APs in the surrounding ventricular tissue. Second of all, consistent with the disappearance of MEPPC clinically observed during exercise, the triggered ventricular APs disappeared at higher pacing frequencies.

Therefore, the model confirms the mechanism by which the Na^+ channel alteration is responsible for the patients' phenotype.

Dilated cardiomyopathy is a secondary consequence of the mutation. *SCN5A* R222Q mutation was already detected in a few patients referred for familial or idiopathic DCM (13,40–42). However, in all previously reported R222Q carriers, DCM was always associated with MEPPC-related ECG patterns. McNair et al. (13) identified 5 *SCN5A* mutations among 338 patients affected by DCM (13). Among them, 2 were carriers of the R222Q mutation and in both cases patients were affected by frequent PVCs (>1,000/h) and NSVT. Morales et al. (42) investigated patients affected by peripartum cardiomyopathy and identified a family carrying the R222Q mutation, affected by DCM (42). In this family, 4 of 6 carriers were also affected by ventricular or supraventricular tachycardia (for 1 patient no information was available). In the families reported here, DCM was diagnosed in 6 individuals, and is very likely a consequence of the arrhythmia, and not directly linked to the mutation. Indeed, 13 patients affected by MEPPC, carriers of the R222Q *SCN5A* mutation, were not affected by DCM. Most importantly, the cardiomyopathy recovered at least partially under antiarrhythmic treatment after having reduced the number of PVCs. The low penetrance of the associated DCM phenotype in these families suggests that the genetic background may play a role in the clinical evolution of the disease as now admitted even for monogenic cardiac arrhythmias (43).

Several other *SCN5A* mutations associated with familial DCM-arrhythmia syndrome have also been described (R814W, D1275N, T220I, and D1595H) (10–12). In these mutation carriers, predominant clinical findings were mainly sinus bradycardia, atrioventricular block, atrial fibrillation, and/or atrial flutter, phenotypes quite different from the MEPPC syndrome. Therefore, our work does not rule out that DCM may be a primary consequence of other *SCN5A* mutations.

Hydroquinidine-based therapy. Because the treatment of the affected patients with hydroquinidine has been proven to be effective on PVCs, we investigated the effects of quinidine on the Na^+ currents and observed equivalent inhibition of WT- and R222Q Nav1.5–mediated currents. Despite the fact that we did not consider the use dependence of quinidine activity (44,45), the multicellular model recapitulates the effects of quinidine on PVCs suppression. Altogether, these results reinforce our hypothesis of MEPPC being the primary consequence of *SCN5A* R222Q mutation. Furthermore, it offers a potentially efficient therapy to limit the symptoms for *SCN5A* R222Q carriers. However, it remains to be shown that the treatment may limit the risk of sudden death.

Acknowledgments

The authors thank André Terzic, University of Minnesota, Minneapolis, Minnesota, for *ABCC9* sequencing and Béatrice Leray, l'institut du thorax, Nantes, France, for expert technical assistance with cell culture.

Reprint requests and correspondence: Dr. Gabriel Laurent, Service de Cardiologie, 2 Boulevard Maréchal De Lattre de Tassigny, 21079 Dijon Cedex, France. E-mail: gabriel.laurent@chu-dijon.fr.

REFERENCES

1. Kaufman ES. Mechanisms and clinical management of inherited channelopathies: long QT syndrome, Brugada syndrome, catecholaminergic polymorphic ventricular tachycardia, and short QT syndrome. Heart Rhythm 2009;6:S51–5.
2. Mohler PJ, Schott JJ, Gramolini AO, et al. Ankyrin-B mutation causes type 4 long-QT cardiac arrhythmia and sudden cardiac death. Nature 2003;421:634–9.
3. Watanabe H, Koopmann TT, Le Scouarnec S, et al. Sodium channel beta1 subunit mutations associated with Brugada syndrome and cardiac conduction disease in humans. J Clin Invest 2008;118:2260–8.

4. Hedley PL, Jorgensen P, Schlamowitz S, et al. The genetic basis of long QT and short QT syndromes: a mutation update. Hum Mutat 2009;30:1486–511.
5. Zimmer T, Surber R. SCN5A channelopathies—an update on mutations and mechanisms. Prog Biophys Mol Biol 2008;98:120–36.
6. Tfelt-Hansen J, Winkel BG, Grunnet M, Jespersen T. Inherited cardiac diseases caused by mutations in the Nav1.5 sodium channel. J Cardiovasc Electrophysiol 2010;21:107–15.
7. Rook MB, Bezzina AC, Groenewegen WA, et al. Human SCN5A gene mutations alter cardiac sodium channel kinetics and are associated with the Brugada syndrome. Cardiovasc Res 1999;44:507–17.
8. Schott JJ, Alshinawi C, Kyndt F, et al. Cardiac conduction defects associate with mutations in SCN5A. Nat Genet 1999;23:20–1.
9. Probst V, Kyndt F, Potet F, et al. Haploinsufficiency in combination with aging causes SCN5A-linked hereditary Lenegre disease. J Am Coll Cardiol 2003;41:643–52.
10. Olson TM, Michels VV, Ballew JD, et al. Sodium channel mutations and susceptibility to heart failure and atrial fibrillation. JAMA 2005; 293:447–54.
11. McNair WP, Ku L, Taylor MR, et al. SCN5A mutation associated with dilated cardiomyopathy, conduction disorder, and arrhythmia. Circulation 2004;110:2163–7.
12. Nguyen TP, Wang DW, Rhodes TH, George AL, Jr. Divergent biophysical defects caused by mutant sodium channels in dilated cardiomyopathy with arrhythmia. Circ Res 2008;102:364–71.
13. McNair WP, Sinagra G, Taylor MR, et al. SCN5A mutations associate with arrhythmic dilated cardiomyopathy and commonly localize to the voltage-sensing mechanism. J Am Coll Cardiol 2011; 57:2160–8.
14. Remme CA, Wilde AA, Bezzina CR. Cardiac sodium channel overlap syndromes: different faces of SCN5A mutations. Trends Cardiovasc Med 2008;18:78–87.
15. Wolf CM, Wang L, Alcalai R, et al. Lamin A/C haploinsufficiency causes dilated cardiomyopathy and apoptosis-triggered cardiac conduction system disease. J Mol Cell Cardiol 2008;44:293–303.
16. Bienengraeber M, Olson TM, Selivanov VA, et al. ABCC9 mutations identified in human dilated cardiomyopathy disrupt catalytic KATP channel gating. Nat Genet 2004;36:382–7.
17. Genin E, Tullio-Pelet A, Begeot F, Lyonnet S, Abel L. Estimating the age of rare disease mutations: the example of Triple-A syndrome. J Med Genet 2004;41:445–9.
18. Allouis M, Le Bouffant F, Wilders R, et al. 14-3-3 is a regulator of the cardiac voltage-gated sodium channel Nav1.5. Circ Res 2006;98: 1538–46.
19. DiFrancesco D, Noble D. A model of cardiac electrical activity incorporating ionic pumps and concentration changes. Philos Trans R Soc Lond B Biol Sci 1985;307:353–98.
20. Iyer V, Mazhari R, Winslow RL. A computational model of the human left-ventricular epicardial myocyte. Biophys J 2004;87:1507–25.
21. Keener J, Sneyd J. Mathematical Physiology. 2nd edition. New York, NY: Springer, 2001.
22. Aslanidi OV, Stewart P, Boyett MR, Zhang H. Optimal velocity and safety of discontinuous conduction through the heterogeneous Purkinje-ventricular junction. Biophys J 2009;97:20–39.
23. Kampmann C, Wiethoff CM, Wenzel A, et al. Normal values of M mode echocardiographic measurements of more than 2000 healthy infants and children in central Europe. Heart 2000;83:667–72.
24. Nogami A, Naito S, Tada H, et al. Demonstration of diastolic and presystolic Purkinje potentials as critical potentials in a macroreentry circuit of verapamil-sensitive idiopathic left ventricular tachycardia. J Am Coll Cardiol 2000;36:811–23.
25. Reithmann C, Hahnefeld A, Ulbrich M, Matis T, Steinbeck G. Different forms of ventricular tachycardia involving the left anterior fascicle in nonischemic cardiomyopathy: critical sites of the reentrant circuit in low-voltage areas. J Cardiovasc Electrophysiol 2009;20: 841–9.
26. Tanner H, Hindricks G, Volkmer M, et al. Catheter ablation of recurrent scar-related ventricular tachycardia using electroanatomical mapping and irrigated ablation technology: results of the prospective multicenter Euro-VT-study. J Cardiovasc Electrophysiol 2010;21:47–53.
27. Imaizumi Y, Giles WR. Quinidine-induced inhibition of transient outward current in cardiac muscle. Am J Physiol 1987;253:H704–8.
28. Wang Z, Fermini B, Nattel S. Effects of flecainide, quinidine, and 4-aminopyridine on transient outward and ultrarapid delayed rectifier currents in human atrial myocytes. J Pharmacol Exp Ther 1995;272: 184–96.
29. Roden DM, Bennett PB, Snyders DJ, Balser JR, Hondeghem LM. Quinidine delays IK activation in guinea pig ventricular myocytes. Circ Res 1988;62:1055–8.
30. Sanchez-Chapula JA, Ferrer T, Navarro-Polanco RA, Sanguinetti MC. Voltage-dependent profile of human ether-a-go-go-related gene channel block is influenced by a single residue in the S6 transmembrane domain. Mol Pharmacol 2003;63:1051–8.
31. Salata JJ, Wasserstrom JA. Effects of quinidine on action potentials and ionic currents in isolated canine ventricular myocytes. Circ Res 1988;62:324–37.
32. Iost N, Virag L, Varro A, Papp JG. Comparison of the effect of class IA antiarrhythmic drugs on transmembrane potassium currents in rabbit ventricular myocytes. J Cardiovasc Pharmacol Ther 2003;8:31–41.
33. Wu L, Guo D, Li H, et al. Role of late sodium current in modulating the proarrhythmic and antiarrhythmic effects of quinidine. Heart Rhythm 2008;5:1726–34.
34. Lopera G, Stevenson WG, Soejima K, et al. Identification and ablation of three types of ventricular tachycardia involving the His-Purkinje system in patients with heart disease. J Cardiovasc Electrophysiol 2004;15:52–8.
35. Rodriguez LM, Smeets JL, Timmermans C, Trappe HJ, Wellens HJ. Radiofrequency catheter ablation of idiopathic ventricular tachycardia originating in the anterior fascicle of the left bundle branch. J Cardiovasc Electrophysiol 1996;7:1211–6.
36. Doppalapudi H, Yamada T, McElderry HT, Plumb VJ, Epstein AE, Kay GN. Ventricular tachycardia originating from the posterior papillary muscle in the left ventricle: a distinct clinical syndrome. Circ Arrhythm Electrophysiol 2008;1:23–9.
37. Kapplinger JD, Tester DJ, Alders M, et al. An international compendium of mutations in the SCN5A-encoded cardiac sodium channel in patients referred for Brugada syndrome genetic testing. Heart Rhythm 2010;7:33–46.
38. Kapplinger JD, Tester DJ, Salisbury BA, et al. Spectrum and prevalence of mutations from the first 2,500 consecutive unrelated patients referred for the FAMILION long QT syndrome genetic test. Heart Rhythm 2009;6:1297–303.
39. Makita N. Phenotypic overlap of cardiac sodium channelopathies: individual-specific or mutation-specific? Circ J 2009;73:810–7.
40. Cheng J, Morales A, Siegfried JD, et al. SCN5A rare variants in familial dilated cardiomyopathy decrease peak sodium current depending on the common polymorphism H558R and common splice variant Q1077del. Clin Transl Sci 2010;3:287–94.
41. Hershberger RE, Parks SB, Kushner JD, et al. Coding sequence mutations identified in MYH7, TNNT2, SCN5A, CSRP3, LBD3, and TCAP from 313 patients with familial or idiopathic dilated cardiomyopathy. Clin Transl Sci 2008;1:21–6.
42. Morales A, Painter T, Li R, et al. Rare variant mutations in pregnancy-associated or peripartum cardiomyopathy. Circulation 2010;121:2176–82.
43. Roden DM. Human genomics and its impact on arrhythmias. Trends Cardiovasc Med 2004;14:112–6.
44. Snyders DJ, Hondeghem LM. Effects of quinidine on the sodium current of guinea pig ventricular myocytes. Evidence for a drug-associated rested state with altered kinetics. Circ Res 1990;66:565–79.
45. Yang T, Roden DM. Extracellular potassium modulation of drug block of IKr. Implications for torsade de pointes and reverse use-dependence. Circulation 1996;93:407–11.

Key Words: arrhythmia ■ Purkinje fibers ■ SCN5A ■ ventricular tachycardia.

APPENDIX

For expanded Methods and Results sections, as well as supplemental tables, figures, and videos, please see the online version of this article.

Multifocal Ectopic Purkinje Premature Contractions: a new SCN5A-related cardiac channelopathy

Gabriel Laurent, MD, PhD, Samuel Saal, MD, Mohamed Yassine Amarouch, PhD, Delphine M Beziau, MSc, Roos FJ Marsman, MSc, Laurence Faivre, MD, PhD, Julien Barc, PhD, Christian Dina, PhD, Geraldine Bertaux, MD, Olivier Barthez, MD, Christel Thauvin-Robinet, MD, PhD, Philippe Charron, MD, PhD, Véronique Fressart, MD, PhD, Alice Maltret, MD, Elisabeth Villain, MD, Estelle Baron, BA, Jean Mérot, PhD, Rodolphe Turpault, PhD, Yves Coudière, PhD, Flavien Charpentier, PhD, Jean Jacques Schott, PhD, Gildas Loussouarn, PhD, Arthur A. M. Wilde, MD, PhD, Jean Eric Wolf, MD, PhD, Isabelle Baró, PhD, Florence Kyndt, PharmD, PhD, Vincent Probst, MD, PhD.

ONLINE DATA SUPPLEMENT

SUPPLEMENTAL METHODS

Mutation analysis

The proband (III.1) of family 1 was screened for mutations in *LMNA* encoding lamin A/C, *ABCC9* encoding SUR2A and SCN5A. All 12 coding exons and intronic junctions of *LMNA* were amplified and scanned using an HRMA/sequencing method (conditions available under request) using the Light-Cycler® 480 High Resolution Melting Master kit according to the manufacturer's instructions (Roche Applied Science, Meylan, France) and further scanned by HRM analysis. PCR products showing divergent HRM profiles were purified and directly sequenced on both strands using the BigDye® Terminator v.3.1 Cycle Sequencing Kit (Applied Biosystems, Forster City, CA). After purification, sequencing products were applied onto an ABI 3730 automatic sequencer (Applied Biosystems). Screening for mutation in *ABCC9* gene was performed as previously described (1).

Screening for mutation in *SCN5A* was performed by a polymerase chain reaction amplification of coding regions and flanking intronic sequences (primers sequences available under requests) followed by bidirectional sequencing of amplicons using the BigDye® Terminator v.3.1 Cycle Sequencing Kit (Applied Biosystems, Forster City, CA. After purification, sequencing products were applied onto on an ABI PRISM 3730 DNA sequence detection system (Applied Biosystems).

Exon 6 of *SCN5A*, which includes the c.665G>A transition, was amplified from genomic DNA of family 1 and 2 members with primers CACCCCCTTTCCTCCTCT and CCAGGCATATCCCTCTAGCC. The purified PCR product was sequenced using BigDye Terminator 3.1 (Applied Biosystems) chemistry.

For family 3, exon 6 of *SCN5A* was amplified from genomic DNA of the proband II-3 and the purified PCR product similarly sequenced. The sequence variant present in all affected family members was further confirmed by digestion with HinfI (New England BioLabs, Beverly, MA). HinfI digests the fragment containing c.665G but does not digest that with c.665A.

Six hundred Caucasian control chromosomes from Human Random Control (HRC) panels were screened for the presence of the c.665G>A transition using HRM (High Resolution Melting) assay on the LightCycler 480 System (Roche) and the same primers.

Haplotype Analysis

To ascertain whether there is a common disease haplotype for the R222Q mutation of the *SCN5A* gene in the two families with MEPT, and estimate the low limit of the most recent common ancestor, 10 microsatellite markers around the *SCN5A* gene (D3S1759, D3S2432, D3S3047, D3S3512, D3S1298, intragenic *SCN5A* marker, D3S3521, D3S3527, D3S3522 and D3S3559) were genotyped in individuals from the 3 families. Haplotype analysis was performed in 12 members of family 1 (9 affected), 3 members of family 2 (2 affected) and 3 members of family 3 (3 affected).

The primer sequences were obtained from Ensembl (www.ensembl.org) except for the intragenic marker. Each marker was amplified by PCR and the sense primers were 5'-end labeled with fluorescence (R6G and R110-dCTP, Perkin Elmer).

PCR was performed under the following conditions: denaturation at 94°C for 3 min; 30 cycles of denaturation at 94°C for 30 sec, annealing at 55°C for 30 sec, and extension at 72°C for 1 min; final extension at 72°C for 10 min. Alleles were submitted to electrophoresis using an ABI PRISM 3730 DNA analyser, (PE Applied Biosystems), with ROX-500 size standard (PE Applied Biosystems). Genotype

analysis was automated using GeneMapper software, version 4.0 (PE Applied Biosystems).

We estimated the age of the mutation using the Genin and collaborators method (2), based on the length of identity by state segments around the mutation. This method identifies the closest markers at which the two affected individuals do not share any allele on either side. The likelihood is built on the number of recombination events between the mutation and the neighboring genetic markers, with a correction through the possibility of mutation. Because we did not have even a single common allele in the haplotypic background of families 1 and 2, we created two dummy markers, with shared common allele by both affected individuals at a recombination fraction θ=0.0001 both upstream and downstream the mutation. Thus, we were aiming at finding a lower threshold to the number of generations to the most recent common ancestor. We adopted a micro-satellite mutation rate of $m=3.10^{-3}$ (using the Stepwise Mutation Model), as proposed in the literature (3). It is noteworthy that the time to the Most Recent Common Ancestor is not necessarily the time to the mutation occurrence. Therefore, our number of generations is also a lower bound for the age of the allele.

Site-directed mutagenesis

Site-directed mutagenesis was performed on pCI-SCN5A (4) using the Quick-Change site-directed mutagenesis kit (Stratagene) according to the manufacturer's instructions. The construct was completely sequenced to ensure that there was no other mutation.

Cellular electrophysiology

The African green monkey kidney fibroblast-like cell line (COS-7) was obtained from the American Type Culture Collection and cultured as previously described (5). Cells were transfected with DNA complexed to JetPEI (Polyplus-tranfection) according to the manufacturer's instructions. Relative DNA concentrations were 10% pCI-Nav1.5 (RefSeq NG_008934.1) WT or R222Q, or 5% of each for the heterozygous condition), 10% pRC-hβ1 (4) and 80% pEGFP (Clontech). The resulting Nav1.5 protein is the splice variant containing H 558 and Q1077 amino acids. At eight hours post-transfection, the cells were isolated and seeded in plastic Petri dishes at low density. At twenty-four hours post-transfection, whole-cell currents were recorded at room temperature using the patch-clamp technique. The cells were continuously superfused with Tyrode solution containing (in mmol/L): NaCl 145, KCl 4, $MgCl_2$ 1, $CaCl_2$ 1, HEPES 5, glucose 5, pH adjusted to 7.4 with NaOH. Wax-coated pipettes (tip resistance: 1.8 to 3 MΩ) were filled with intracellular medium containing (in mmol/L): NaCl 10, CsCl 64.5, aspartic acid 70.5, HEPES 5, pH adjusted to 7.2 with CsOH. During data recording, the studied cell was locally superfused with extracellular medium containing (in mmol/L): NaCl 145, CsCl 4, $CaCl_2$ 1, $MgCl_2$ 1, HEPES 5, glucose 5, pH adjusted to 7.4 with NaOH with 30 µM quinidine or 30 µM tetrodotoxin (TTX) when needed. All products were purchased from Sigma, except TTX, provided by Tocris Bioscience. Stimulation, data recording through an A/D converter (Tecmar TM100 Labmaster, Scientific Solutions; 5 kHz filtering), and analysis were performed with Acquis1 software (Bio-Logic). All current measurements were normalized using the cell capacitance. Capacitance and series resistances were compensated (60-70% compensation) to obtain minimal contribution of capacitive transients using an Axopatch 200A amplifier (Axon Instruments, Inc).

Mathematical modeling of ventricular and Purkinje action potentials

Single-cell models

The same strategy was used for both models of the human Purkinje cells (6) and left-ventricular myocytes (7). The equations corresponding to the Na^+ current were iteratively modified to reproduce the relative variation of 8 parameters due to the R222Q mutation (i.e. peak amplitude at -20 mV, half-activation potential, activation slope, time to peak at -20 mV, half-inactivation potential, inactivation slope and the kinetics of inactivation at -35 mV and recovery from inactivation at -100 mV). The other currents generating the action potential were not modified.

In the Purkinje cell model, the effects of the R222Q mutation were simulated by (i) modifying α_m and β_m to recapitulate the shift in the activation curve and (ii) modifying β_h to recapitulate the shift in the inactivation with no change in the recovery from inactivation. The WT and R222Q Na^+ current formulations followed the DiFrancesco and Noble model (6) as such:

WT	**R222Q**
α_h = 20 x exp(-0.125 x (V + 75))	α_h = 20 x exp(-0.125*(V + 75))
β_h = 2000/(320 x exp(-0.1x (V + 75))+1)	β_h = 2000/(320 x exp(-0.1 x (V + 75 + **10**))+1)
α_m = 200 x (V+ 41)/(1-exp(-0.1 x (V + 41)))	α_m = 200 x (V+ 41+**shift**)/(1-exp(-0.1 x (V + 41 + **shift**)))
β_m = 8000 x exp(-0.056 x (V + 66))	β_m = 8000 x exp(-0.056 x (V + 66 + **shift**))

where “shift” was set to 12 to best fit the shift in the activation curve. This value was also used in the multicellular model. But interestingly, in the unicellular model, an excessive Na^+ window current prevented repolarization and the value had to be decreased to 9 to observe an action potential.

To mimic the heterozygous condition, the Na^+ current resulted from the summation of half the WT current and half the R222Q current.

In the ventricular cell model, the effects of the R222Q mutation were simulated (i) by modifying all the forward transitions ($\alpha,\beta,\gamma,\gamma\gamma,\eta$) to recapitulate the shift in the activation curve and (ii) by decreasing the inactivation/activation coupling factor to recapitulate the smaller shift in the inactivation curve with no change in the recovery from inactivation kinetics. The WT and R222Q Na^+ current formulation followed model (7) as such:

WT	**R222Q**
α = 26 x exp(0.011 x V)	η = 26 x exp(0.011 x (V**+11**))
β = 0.036 x exp(-0.090 x V)	β = 0.036 x exp(-0.090 x (V**+11**))
γ = 590 x exp(0.110 x V)	γ = 590 x exp(0.110 x (V**+11**))
$\gamma\gamma$ = 2.6 x exp(0.030 x V)	$\gamma\gamma$ = 2.6 x exp(0.030 x (V**+11**))
η = 26 x exp(0.084 x V)	η = 26 x exp(0.084 x (V**+11**))
a = 1.4004	a = **1.21**

The other transition constants were not changed.

Both the Purkinje and ventricular Na^+ currents were modeled with Model Maker v4.0 (AP Benson, Wallingford, UK) and with a home-made program running on C++. The action potentials (APs) were modeled with a home-made program running on C++.

Multicellular model

Both models of the human left-ventricular subepicardial myocytes and Purkinje cells were incorporated in a multicellular model. In this model, the propagation of the electrical waves in the cardiac tissues was described by a monodomain model (8). The membrane potential is described by a variable V following the partial differential equation:

$$A_m C_m \frac{\partial V}{\partial t} - \nabla.(D\nabla V) = A_m I_{ion}$$

Where t is the time in s, V is the transmembrane potential in mV, Am is the ratio of membrane surface per cell volume unit [1e3 cm^{-1}], Cm is the membrane capacitance per surface unit [1e-3 $mF.cm^{-2}$], and D is the average electrical conductivity of the tissue [20 $mS.cm^{-1}$ in Purkinje cells, and 1.3 $mS.cm^{-1}$ in ventricular cells]. The ionic current per surface unit I_{ion} [$\mu A.cm^{-2}$] was computed according to the models introduced above. The values of D were adjusted to obtain a propagation speed in the range of around 180 cm/s in the Purkinje system, and 90 cm/s in the ventricle. The numerical simulations were performed on a simplified 2D slice model described previously (9). The pacing site was located at the proximal part of the Purkinje fiber (see Figure. 5). The ordinary differential equations of the ionic model were integrated by a mixed explicit-implicit method, with a 1-µs step. To mimic the quinidine effects, I_{Na}, I_{to} and I_{Kr} were reduced based on the results of Wu (10;11;12) for I_{Na} and I_{Kr}, and Wang (13) for I_{to}. For the first test, we chose 10 µM quinidine, the maximal therapeutic dose *i.e.* preserving 50% I_{Na}, 30% I_{Kr} (12) and 30% I_{to} (13). Assuming that the mimicked doses were in the linear zone of the concentration-dose relationship for inhibition of the different ion currents, we also computed the consequences of preserving 75% I_{Na} and 45% I_{Kr} and I_{to} and of 85% and 50%, respectively. The computations were performed on a mesh with 2225 vertices using the cluster from the *Centre de Calcul Intensif des Pays de Loire*.

SUPPLEMENTAL RESULTS

Haplotype analysis

The alleles of 4 SCN5A flanking markers (D3S3512, D3S1298, D3S3521, D3S3527) and of the intragenic SCN5A marker were shared by the affected individuals in each family, but differed between the families 1 and 2, and 2 and 3. These results indicate that the cosegregating haplotype was different in each of these families, suggesting independent mutations origin. Using the method of Genin and collaborators, we found at least 126 generations from a hypothetical most recent common ancestor (95% confidence interval from 37 to 464 generations) for families 1 and 2. Such an ancient common origin does not fit with the fact that the observed mutation allele frequency is below 9.10^{-3} (higher bound confidence interval for no observation in 300 control individuals). The probands of families 1 and 3 shared at least two frequent microsatellite alleles (D3S1298 and D3S3512) but not the rare intragenic one. As a conclusion, families 1 and 3 may be at least 28-generation distantly related.

Computer modeling shows that ventricular cells better tolerate the mutation than Purkinje cells.

To get insights on the R222Q mutation effect on the action potentials (APs) at a cellular scale, we carried out computer simulations to evaluate the impact of the mutation on the Na^+ current in unicellular models of Purkinje and ventricular cells (6-7). The models modifications operated to mimic the mutation-induced changes in the Na^+ current have been detailed in the Supplemental Methods section. The relative shift in activation and inactivation curves in the heterozygous state, as well as all other changes of the biophysical parameters were compared to those experimentally measured in heterozygous state. Despite that the transfected cell population may be a mixture of cells expressing mainly WT, R222Q or both Nav1.5 channels, the experimental ‘heterozygous’ parameters were successfully reproduced in both the Purkinje (Supplemental Figure 5B) and ventricular (Supplemental Figure 5C) cell

models. Interestingly, when the equations mimicking the heterozygous state of the patients were introduced into the ventricular cell model, minor changes in AP morphology were observed (Supplemental Figure 6). Conversely, when the equations mimicking the heterozygous state were introduced in the Purkinje cell model, the effect was drastic: AP could not be induced (not shown). AP could be generated only if the shift in the activation curve was reduced (4 instead of 6 mV), in order to limit the Na^+ current increase (Supplemental Figure 6). But AP morphology was still highly affected. This disappeared at higher pacing rates, consistent with PVCs disappearing during exercise (Supplemental Figure 6).

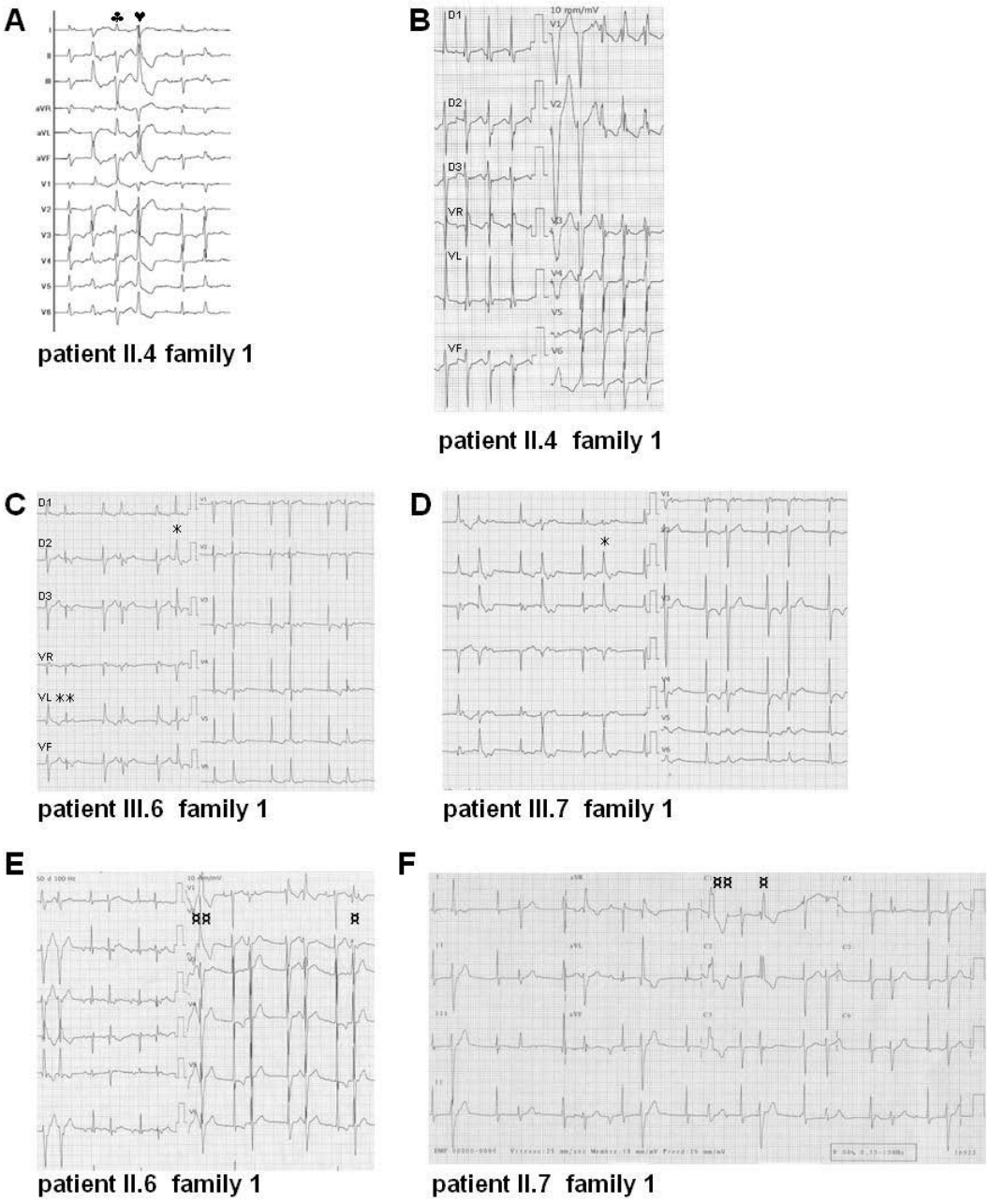

Supplemental Figure 1. Representative ECGs of family 1. Some patients (**A**) had PVC with RBBB patterns and alternant extreme variations in the axis from right (♣) to left (♥), from beat to beat. Recurrent monomorphic non-sustained ventricular tachyarrhythmia (NSVT) (**B**), and slightly polymorphic NSVT were also observed. In some patients, PVCs were relatively narrow QRS complexes (**C-D**), very similar to either sinus or junctional complexes with slight variations in the left axis from +60° (*) to -30° (**). In some patients (**E-F**), PVCs had RBBB patterns with various widths from relatively narrow (¤) to wide QRS complexes (¤¤).

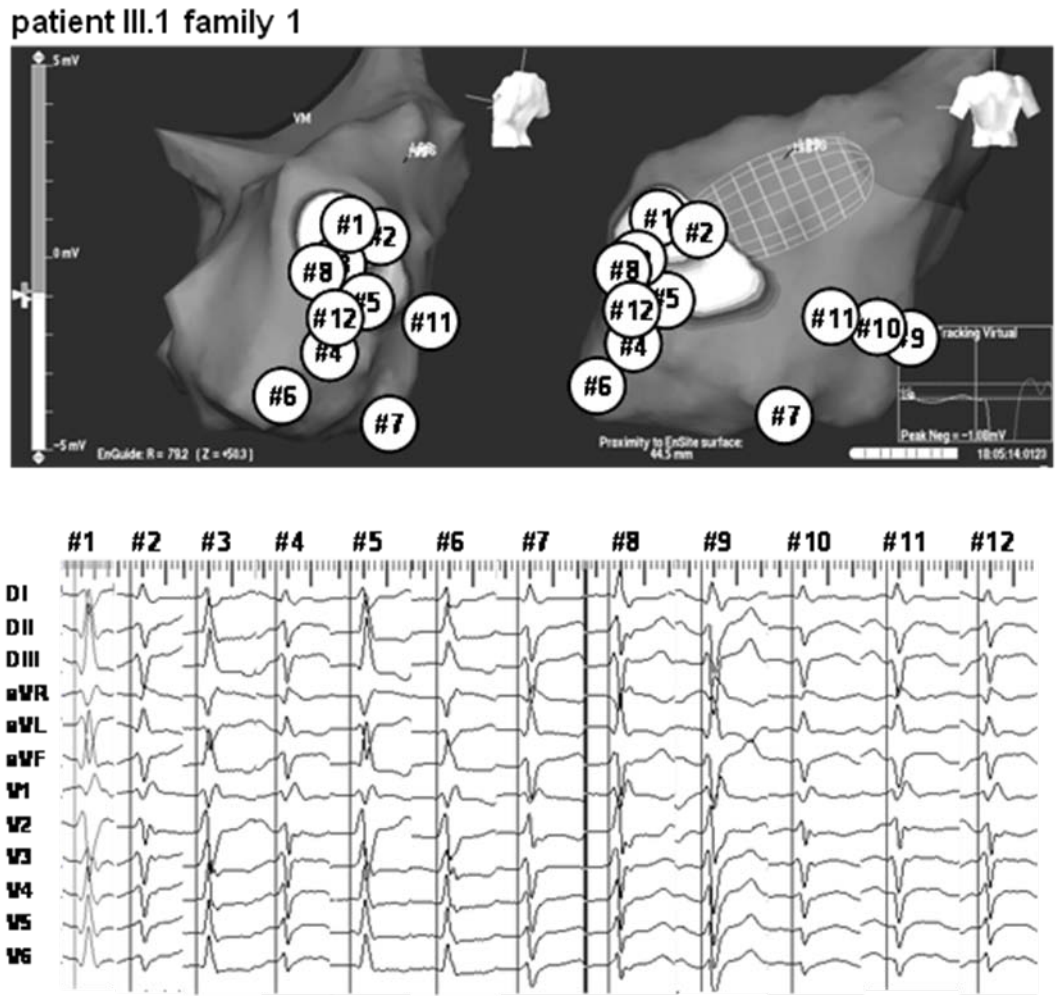

Supplemental Figure 2. Endocardial electroanatomic mapping of the left ventricle. Activation mapping of 12 different PVCs in patient III.1 (family 1). A Multi-array balloon (NavX system) helped us to pinpoint the precise location of ectopic foci along the anterior and posterior regions of the left ventricle corresponding to the extension of the left anterior and posterior fascicles.

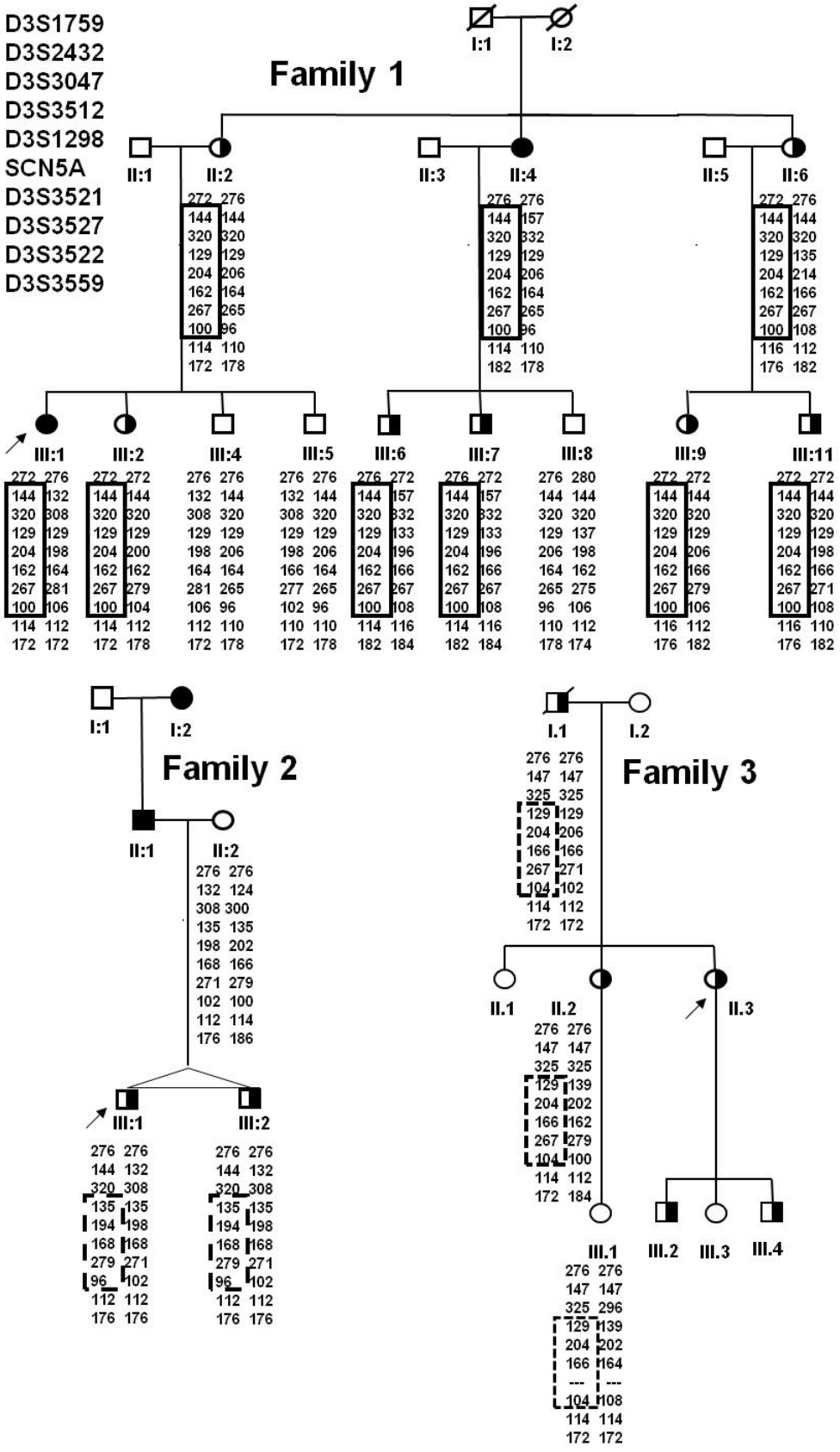

Supplemental Figure 3. Haplotype analysis of chromosome 3 in selected members for families 1, 2 and 3. Females are represented by circles and males are

represented by squares. Members affected with arrhythmia are indicated with a half-filled symbol. Members affected with arrhythmia and dilated cardiomyopathy (DCM) are indicated in black. Ten microsatellite markers (D3S1759, D3S2432, D3S3047, D3S3512, D3S1298, intragenic *SCN5A* marker, D3S3521, D3S3527, D3S3522 and D3S3559) spanning the region of chromosome 3 where the *SCN5A* gene lies, were analyzed. The disease-associated haplotype is indicated by a black frame. The disease haplotype in family 2 differed from that in family 1, showing that the R222Q mutation has arisen independently in these two families. Common alleles of two microsatellites are shared by families 1 and 3 implying a possible most recent common ancestor at least 28 generations earlier.

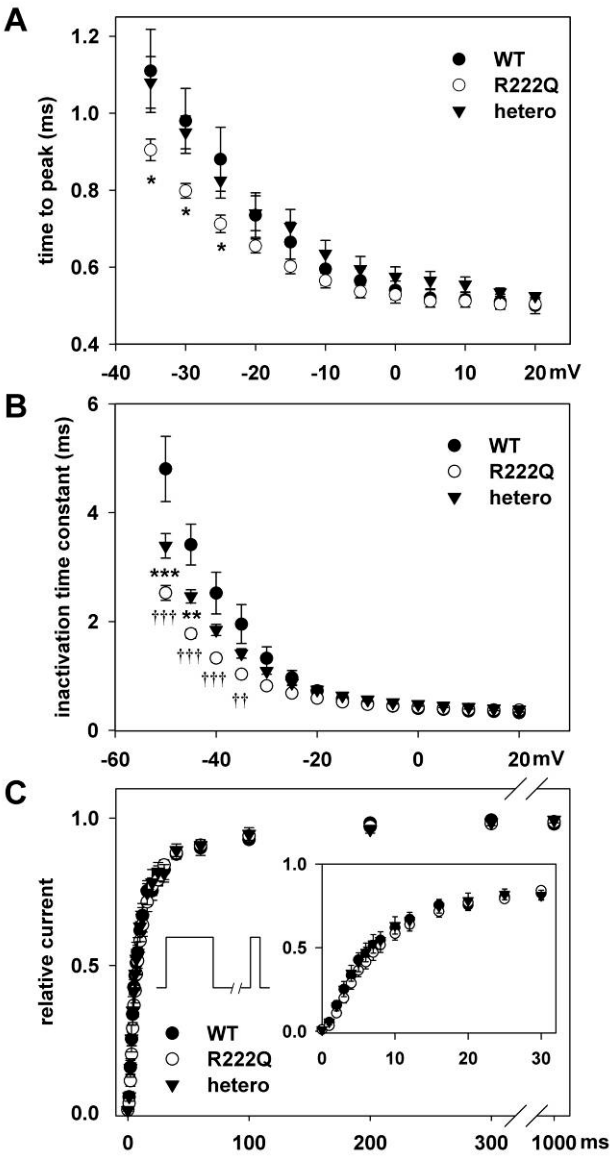

Supplemental Figure 4. Experimental effects of R222Q mutation on Nav1.5 channel in COS-7 cells. (**A**) Na^+ current time-to-peak values were used to evaluate the activation kinetics. Same transfection and voltage protocol as in Figure 4A. Tukey test: *, p<0.05 *vs* WT. (**B**) Accelerated inactivation in the presence of the R222Q mutation. Inactivation time constants were measured by fitting the inactivation phase of the Na^+ current to a single exponential equation. Tukey test: Heterozygous *vs.* WT, **: p<0.01, ***: p <0.001; R222Q *vs* WT, †: p<0.05, †††: p<0.001. (**C**) Recovery from inactivation was measured using a twin-pulse protocol (left inset: holding potential: –100 mV, 100-ms depolarization to -20 mV, back to -100 mV for 0 to 1000-ms delay before test pulse to -20 mV, frequency:0.1 Hz). Right inset: same as main graph for short delays.

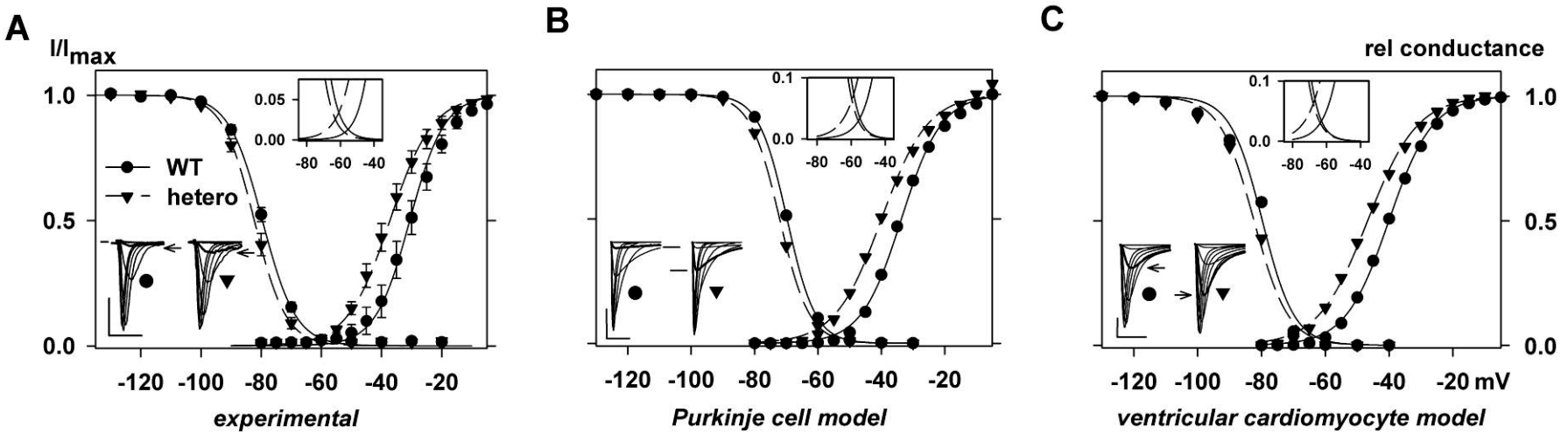

Supplemental Figure 5. (**A**) Superimposed activation and inactivation curves of WT (circles, solid line) and heterozygous (triangles, dashed line) channels obtained experimentally. Bottom inset: superimposed Na^+ current recordings using the same voltage protocol as in figure 4. Scale bars: 2 ms, 1000 pA. Top inset: increase of the predicted voltage window current in the presence of the mutation. (**B**) and (**C**) Simulated curves of WT (circles, solid line) and heterozygous (triangles, dashed line) channels; activation and inactivation in Purkinje cell (B) and (C) ventricular cardiomyocyte models. Bottom insets, simulated Na^+ currents as in A. Scale bars: 1 ms, 100 pA (B) and 5 ms, 100 pA (C). Top insets, as in A.

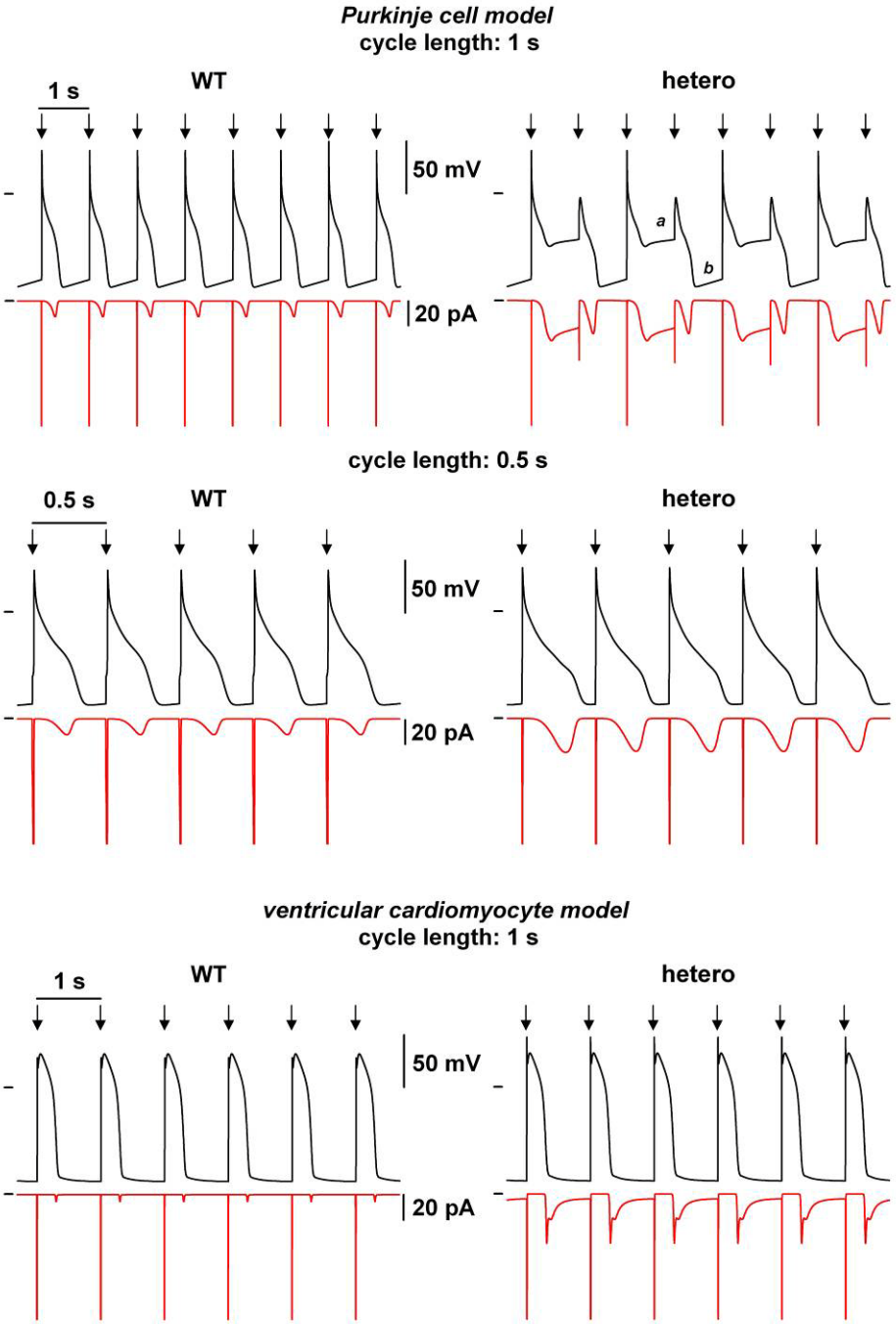

Supplemental Figure 6. Effects of the R222Q mutation on Purkinje (top) and ventricular (bottom) cell action potentials (APs) and Na^+ current obtained in the single-cell model. Simulated AP (black) and late Na^+ current (red) in WT (left) and heterozygous (right) conditions at the indicated cycle lengths. Arrows: external stimulus.

Supplemental movies

Simulation of the AP propagation from a Purkinje fiber to ventricular tissue (dimensions and stimulation shown in Figure 4), in WT (a) and heterozygous (b) conditions at cycle length of 1 s (A) and 0.5 s (B).

Supplemental Table 1: Effects of R222Q mutation on Nav1.5 biophysical parameters.

	current density	activation		inactivation		recovery from inactivation	window current		
	peak at –20 mV (pA/pF)	$V_{1/2}$ (mV)	k (mV)	$V_{1/2}$ (mV)	k (mV)	$t_{1/2}$ (ms)	g_{max} (pS/pF)	E_{max} (mV)	AUC (a.u.)
WT	–205.8±29.3 (36)	–30.6±2.1 (9)	5.7±0.3 (9)	–79.6±0.7 (10)	5.6±0.2 (10)	7.6±0.6 (6)	15.9±2.6 (13)	-42.8±0.5 (12)	29.9±3.9 (13)
heterozygous	–196.5±17.6 (48)	–37.2±1.6* (9)	7.1±0.3** (9)	–82.2±1* (9)	5.3±0.1 (9)	7.9±1.1 (8)	-	-	-
R222Q	–250.4±24.8 (44)	–42.3±1.0*** (11)	6.5±0.4 (11)	–84.6±0.7*** (8)	4.8±0.2** (8)	8.8±0.9 (8)	19.1±2.0 (14)	-58.6±1.1*** (14)	55.2±7.6** (14)

(n): number of cells; *: p<0.05; **: p<0.01; ***: p<0.001 *vs.* WT; $V_{1/2}$ and k; voltage for half-activation or -inactivation of the Na^+ current and slope; $t_{1/2}$: time to reach 50% recovery of the Na^+ current; g_{max}: maximal TTX-sensitive conductance recorded during a depolarizing-voltage ramp as in Supplemental Figure 4; E_{max}: potential at which the maximum conductance was measured. AUC: area under curve calculated on current density/membrane potential relationship; a.u.: arbitrary unit.

Supplemental Table 2: Effects of quinidine on WT and R222Q Nav1.5 currents.

		current density	window current
		peak at –20 mV (pA/pF)	**I_{max} (pA/pF)**
WT	**control**	–136.0±28.5 (12)	–1.87±0.42 (7)
	30 µM quinidine	–76.7±15.2***	–0.74±0.16*
R222Q	**control**	–123.3±20.1 (10)	–2.54±0.41 (6)
	30 µM quinidine	–63.9±10.5***	–1.17±0.12**

(n): number of cells; paired t-test: *: p<0.05; **: p<0.01; ***: p<0.001 *vs.* control; window current: TTX-sensitive (30 µM) current elicited by a depolarizing-voltage ramp; I_{max}: current density measured when the TTX-sensitive conductance is maximal (*i.e.* at -43 mV and -59 mV for WT and R222Q, respectively).

SUPPLEMENTAL REFERENCES

1 Bienengraeber M, Olson TM, Selivanov VA, Kathmann EC, O'Cochlain F, Gao F, Karger AB, Ballew JD, Hodgson DM, Zingman LV, Pang YP, Alekseev AE, Terzic A. ABCC9 mutations identified in human dilated cardiomyopathy disrupt catalytic KATP channel gating. Nat Genet. 2004;36:382-387.

2 Genin E, Tullio-Pelet A, Begeot F et al. Estimating the age of rare disease mutations: the example of Triple-A syndrome. J Med Genet 2004;41:445-449.

3 Brinkmann B, Klintschar M, Neuhuber F et al. Mutation rate in human microsatellites: influence of the structure and length of the tandem repeat. Am J Hum Genet 1998;62:1408-1415.

4 Kyndt F, Probst V, Potet F et al. Novel SCN5A mutation leading either to isolated cardiac conduction defect or Brugada syndrome in a large French family. Circulation 2001;104:3081-3086.

5 Loussouarn G, Park KH, Bellocq C et al. Phosphatidylinositol-4,5-bisphosphate, PIP2, controls KCNQ1/KCNE1 voltage-gated potassium channels: a functional homology between voltage-gated and inward rectifier K+ channels. EMBO J 2003;22:5412-5421.

6 DiFrancesco D, Noble D. A model of cardiac electrical activity incorporating ionic pumps and concentration changes. Philos Trans R Soc Lond B Biol Sci 1985;307:353-398.

7 Iyer V, Mazhari R, Winslow RL. A computational model of the human left-ventricular epicardial myocyte. Biophys J 2004;87:1507-1525.

8 Keener J, Sneyd J. Mathematical Physiology , 2nd edition. Springer, 2001.

9 Aslanidi OV, Stewart P, Boyett MR et al. Optimal velocity and safety of discontinuous conduction through the heterogeneous Purkinje-ventricular junction. Biophys J 2009;97:20-39.

10 Roden DM, Bennett PB, Snyders DJ et al. Quinidine delays IK activation in guinea pig ventricular myocytes. Circ Res 1988;62:1055-1058.

11 Sanchez-Chapula JA, Ferrer T, Navarro-Polanco RA et al. Voltage-dependent profile of human ether-a-go-go-related gene channel block is influenced by a

single residue in the S6 transmembrane domain. Mol Pharmacol 2003;63:1051-1058.

12 Wu L, Guo D, Li H et al. Role of late sodium current in modulating the proarrhythmic and antiarrhythmic effects of quinidine. Heart Rhythm 2008;5:1726-1734.

13 Wang Z, Fermini B, Nattel S. Effects of flecainide, quinidine, and 4-aminopyridine on transient outward and ultrarapid delayed rectifier currents in human atrial myocytes. J Pharmacol Exp Ther 1995;272:184-196.

Multifocal Ectopic Purkinje Premature Contractions: a new SCN5A-related cardiac channelopathy

Gabriel Laurent, MD, PhD, Samuel Saal, MD, Mohamed Yassine Amarouch, PhD, Delphine M Beziau, MSc, Roos FJ Marsman, MSc, Laurence Faivre, MD, PhD, Julien Barc, PhD, Christian Dina, PhD, Geraldine Bertaux, MD, Olivier Barthez, MD, Christel Thauvin-Robinet, MD, PhD, Philippe Charron, MD, PhD, Véronique Fressart, MD, PhD, Alice Maltret, MD, Elisabeth Villain, MD, Estelle Baron, BA, Jean Mérot, PhD, Rodolphe Turpault, PhD, Yves Coudière, PhD, Flavien Charpentier, PhD, Jean Jacques Schott, PhD, Gildas Loussouarn, PhD, Arthur A. M. Wilde, MD, PhD, Jean Eric Wolf, MD, PhD, Isabelle Baró, PhD, Florence Kyndt, PharmD, PhD, Vincent Probst, MD, PhD.

ONLINE DATA SUPPLEMENT

SUPPLEMENTAL METHODS

Mutation analysis

The proband (III.1) of family 1 was screened for mutations in *LMNA* encoding lamin A/C, *ABCC9* encoding SUR2A and SCN5A. All 12 coding exons and intronic junctions of *LMNA* were amplified and scanned using an HRMA/sequencing method (conditions available under request) using the Light-Cycler® 480 High Resolution Melting Master kit according to the manufacturer's instructions (Roche Applied Science, Meylan, France) and further scanned by HRM analysis. PCR products showing divergent HRM profiles were purified and directly sequenced on both strands using the BigDye® Terminator v.3.1 Cycle Sequencing Kit (Applied Biosystems, Forster City, CA). After purification, sequencing products were applied onto an ABI 3730 automatic sequencer (Applied Biosystems). Screening for mutation in *ABCC9* gene was performed as previously described (1).

Screening for mutation in *SCN5A* was performed by a polymerase chain reaction amplification of coding regions and flanking intronic sequences (primers sequences available under requests) followed by bidirectional sequencing of amplicons using the BigDye® Terminator v.3.1 Cycle Sequencing Kit (Applied Biosystems, Forster City, CA. After purification, sequencing products were applied onto on an ABI PRISM 3730 DNA sequence detection system (Applied Biosystems).

Exon 6 of *SCN5A*, which includes the c.665G>A transition, was amplified from genomic DNA of family 1 and 2 members with primers CACCCCCTTTCCTCCTCT and CCAGGCATATCCCTCTAGCC. The purified PCR product was sequenced using BigDye Terminator 3.1 (Applied Biosystems) chemistry.

For family 3, exon 6 of *SCN5A* was amplified from genomic DNA of the proband II-3 and the purified PCR product similarly sequenced. The sequence variant present in all affected family members was further confirmed by digestion with HinfI (New England BioLabs, Beverly, MA). HinfI digests the fragment containing c.665G but does not digest that with c.665A.

Six hundred Caucasian control chromosomes from Human Random Control (HRC) panels were screened for the presence of the c.665G>A transition using HRM (High Resolution Melting) assay on the LightCycler 480 System (Roche) and the same primers.

Haplotype Analysis

To ascertain whether there is a common disease haplotype for the R222Q mutation of the *SCN5A* gene in the two families with MEPT, and estimate the low limit of the most recent common ancestor, 10 microsatellite markers around the *SCN5A* gene (D3S1759, D3S2432, D3S3047, D3S3512, D3S1298, intragenic *SCN5A* marker, D3S3521, D3S3527, D3S3522 and D3S3559) were genotyped in individuals from the 3 families. Haplotype analysis was performed in 12 members of family 1 (9 affected), 3 members of family 2 (2 affected) and 3 members of family 3 (3 affected).

The primer sequences were obtained from Ensembl (www.ensembl.org) except for the intragenic marker. Each marker was amplified by PCR and the sense primers were 5'-end labeled with fluorescence (R6G and R110-dCTP, Perkin Elmer).

PCR was performed under the following conditions: denaturation at 94°C for 3 min; 30 cycles of denaturation at 94°C for 30 sec, annealing at 55°C for 30 sec, and extension at 72°C for 1 min; final extension at 72°C for 10 min. Alleles were submitted to electrophoresis using an ABI PRISM 3730 DNA analyser, (PE Applied Biosystems), with ROX-500 size standard (PE Applied Biosystems). Genotype

analysis was automated using GeneMapper software, version 4.0 (PE Applied Biosystems).

We estimated the age of the mutation using the Genin and collaborators method (2), based on the length of identity by state segments around the mutation. This method identifies the closest markers at which the two affected individuals do not share any allele on either side. The likelihood is built on the number of recombination events between the mutation and the neighboring genetic markers, with a correction through the possibility of mutation. Because we did not have even a single common allele in the haplotypic background of families 1 and 2, we created two dummy markers, with shared common allele by both affected individuals at a recombination fraction θ=0.0001 both upstream and downstream the mutation. Thus, we were aiming at finding a lower threshold to the number of generations to the most recent common ancestor. We adopted a micro-satellite mutation rate of $m=3.10^{-3}$ (using the Stepwise Mutation Model), as proposed in the literature (3). It is noteworthy that the time to the Most Recent Common Ancestor is not necessarily the time to the mutation occurrence. Therefore, our number of generations is also a lower bound for the age of the allele.

Site-directed mutagenesis

Site-directed mutagenesis was performed on pCI-SCN5A (4) using the Quick-Change site-directed mutagenesis kit (Stratagene) according to the manufacturer's instructions. The construct was completely sequenced to ensure that there was no other mutation.

Cellular electrophysiology

The African green monkey kidney fibroblast-like cell line (COS-7) was obtained from the American Type Culture Collection and cultured as previously described (5). Cells were transfected with DNA complexed to JetPEI (Polyplus-tranfection) according to the manufacturer's instructions. Relative DNA concentrations were 10% pCI-Nav1.5 (RefSeq NG_008934.1) WT or R222Q, or 5% of each for the heterozygous condition), 10% pRC-hβ1 (4) and 80% pEGFP (Clontech). The resulting Nav1.5 protein is the splice variant containing H 558 and Q1077 amino acids. At eight hours post-transfection, the cells were isolated and seeded in plastic Petri dishes at low density. At twenty-four hours post-transfection, whole-cell currents were recorded at room temperature using the patch-clamp technique. The cells were continuously superfused with Tyrode solution containing (in mmol/L): NaCl 145, KCl 4, $MgCl_2$ 1, $CaCl_2$ 1, HEPES 5, glucose 5, pH adjusted to 7.4 with NaOH. Wax-coated pipettes (tip resistance: 1.8 to 3 MΩ) were filled with intracellular medium containing (in mmol/L): NaCl 10, CsCl 64.5, aspartic acid 70.5, HEPES 5, pH adjusted to 7.2 with CsOH. During data recording, the studied cell was locally superfused with extracellular medium containing (in mmol/L): NaCl 145, CsCl 4, $CaCl_2$ 1, $MgCl_2$ 1, HEPES 5, glucose 5, pH adjusted to 7.4 with NaOH with 30 µM quinidine or 30 µM tetrodotoxin (TTX) when needed. All products were purchased from Sigma, except TTX, provided by Tocris Bioscience. Stimulation, data recording through an A/D converter (Tecmar TM100 Labmaster, Scientific Solutions; 5 kHz filtering), and analysis were performed with Acquis1 software (Bio-Logic). All current measurements were normalized using the cell capacitance. Capacitance and series resistances were compensated (60-70% compensation) to obtain minimal contribution of capacitive transients using an Axopatch 200A amplifier (Axon Instruments, Inc).

Mathematical modeling of ventricular and Purkinje action potentials

Single-cell models

The same strategy was used for both models of the human Purkinje cells (6) and left-ventricular myocytes (7). The equations corresponding to the Na^+ current were iteratively modified to reproduce the relative variation of 8 parameters due to the R222Q mutation (i.e. peak amplitude at -20 mV, half-activation potential, activation slope, time to peak at -20 mV, half-inactivation potential, inactivation slope and the kinetics of inactivation at -35 mV and recovery from inactivation at -100 mV). The other currents generating the action potential were not modified.

In the Purkinje cell model, the effects of the R222Q mutation were simulated by (i) modifying α_m and β_m to recapitulate the shift in the activation curve and (ii) modifying β_h to recapitulate the shift in the inactivation with no change in the recovery from inactivation. The WT and R222Q Na^+ current formulations followed the DiFrancesco and Noble model (6) as such:

WT	**R222Q**
α_h = 20 x exp(-0.125 x (V + 75))	α_h = 20 x exp(-0.125*(V + 75))
β_h = 2000/(320 x exp(-0.1x (V + 75))+1)	β_h = 2000/(320 x exp(-0.1 x (V + 75 + **10**))+1)
α_m = 200 x (V+ 41)/(1-exp(-0.1 x (V + 41)))	α_m = 200 x (V+ 41+**shift**)/(1-exp(-0.1 x (V + 41 + **shift**)))
β_m = 8000 x exp(-0.056 x (V + 66))	β_m = 8000 x exp(-0.056 x (V + 66 + **shift**))

where “shift” was set to 12 to best fit the shift in the activation curve. This value was also used in the multicellular model. But interestingly, in the unicellular model, an excessive Na^+ window current prevented repolarization and the value had to be decreased to 9 to observe an action potential.

To mimic the heterozygous condition, the Na^+ current resulted from the summation of half the WT current and half the R222Q current.

In the ventricular cell model, the effects of the R222Q mutation were simulated (i) by modifying all the forward transitions ($\alpha,\beta,\gamma,\gamma\gamma,\eta$) to recapitulate the shift in the activation curve and (ii) by decreasing the inactivation/activation coupling factor to recapitulate the smaller shift in the inactivation curve with no change in the recovery from inactivation kinetics. The WT and R222Q Na^+ current formulation followed model (7) as such:

WT	**R222Q**
α = 26 x exp(0.011 x V)	η = 26 x exp(0.011 x (V**+11**))
β = 0.036 x exp(-0.090 x V)	β = 0.036 x exp(-0.090 x (V**+11**))
γ = 590 x exp(0.110 x V)	γ = 590 x exp(0.110 x (V**+11**))
$\gamma\gamma$ = 2.6 x exp(0.030 x V)	$\gamma\gamma$ = 2.6 x exp(0.030 x (V**+11**))
η = 26 x exp(0.084 x V)	η = 26 x exp(0.084 x (V**+11**))
a = 1.4004	a = **1.21**

The other transition constants were not changed.

Both the Purkinje and ventricular Na^+ currents were modeled with Model Maker v4.0 (AP Benson, Wallingford, UK) and with a home-made program running on C++. The action potentials (APs) were modeled with a home-made program running on C++.

Multicellular model

Both models of the human left-ventricular subepicardial myocytes and Purkinje cells were incorporated in a multicellular model. In this model, the propagation of the electrical waves in the cardiac tissues was described by a monodomain model (8). The membrane potential is described by a variable V following the partial differential equation:

$$A_m C_m \frac{\partial V}{\partial t} - \nabla.(D\nabla V) = A_m I_{ion}$$

Where t is the time in s, V is the transmembrane potential in mV, Am is the ratio of membrane surface per cell volume unit [1e3 cm^{-1}], Cm is the membrane capacitance per surface unit [1e-3 $mF.cm^{-2}$], and D is the average electrical conductivity of the tissue [20 $mS.cm^{-1}$ in Purkinje cells, and 1.3 $mS.cm^{-1}$ in ventricular cells]. The ionic current per surface unit I_{ion} [$\mu A.cm^{-2}$] was computed according to the models introduced above. The values of D were adjusted to obtain a propagation speed in the range of around 180 cm/s in the Purkinje system, and 90 cm/s in the ventricle. The numerical simulations were performed on a simplified 2D slice model described previously (9). The pacing site was located at the proximal part of the Purkinje fiber (see Figure. 5). The ordinary differential equations of the ionic model were integrated by a mixed explicit-implicit method, with a 1-µs step. To mimic the quinidine effects, I_{Na}, I_{to} and I_{Kr} were reduced based on the results of Wu (10;11;12) for I_{Na} and I_{Kr}, and Wang (13) for I_{to}. For the first test, we chose 10 µM quinidine, the maximal therapeutic dose *i.e.* preserving 50% I_{Na}, 30% I_{Kr} (12) and 30% I_{to} (13). Assuming that the mimicked doses were in the linear zone of the concentration-dose relationship for inhibition of the different ion currents, we also computed the consequences of preserving 75% I_{Na} and 45% I_{Kr} and I_{to} and of 85% and 50%, respectively. The computations were performed on a mesh with 2225 vertices using the cluster from the *Centre de Calcul Intensif des Pays de Loire*.

SUPPLEMENTAL RESULTS

Haplotype analysis

The alleles of 4 SCN5A flanking markers (D3S3512, D3S1298, D3S3521, D3S3527) and of the intragenic SCN5A marker were shared by the affected individuals in each family, but differed between the families 1 and 2, and 2 and 3. These results indicate that the cosegregating haplotype was different in each of these families, suggesting independent mutations origin. Using the method of Genin and collaborators, we found at least 126 generations from a hypothetical most recent common ancestor (95% confidence interval from 37 to 464 generations) for families 1 and 2. Such an ancient common origin does not fit with the fact that the observed mutation allele frequency is below 9.10^{-3} (higher bound confidence interval for no observation in 300 control individuals). The probands of families 1 and 3 shared at least two frequent microsatellite alleles (D3S1298 and D3S3512) but not the rare intragenic one. As a conclusion, families 1 and 3 may be at least 28-generation distantly related.

Computer modeling shows that ventricular cells better tolerate the mutation than Purkinje cells.

To get insights on the R222Q mutation effect on the action potentials (APs) at a cellular scale, we carried out computer simulations to evaluate the impact of the mutation on the Na^+ current in unicellular models of Purkinje and ventricular cells (6-7). The models modifications operated to mimic the mutation-induced changes in the Na^+ current have been detailed in the Supplemental Methods section. The relative shift in activation and inactivation curves in the heterozygous state, as well as all other changes of the biophysical parameters were compared to those experimentally measured in heterozygous state. Despite that the transfected cell population may be a mixture of cells expressing mainly WT, R222Q or both Nav1.5 channels, the experimental ‘heterozygous’ parameters were successfully reproduced in both the Purkinje (Supplemental Figure 5B) and ventricular (Supplemental Figure 5C) cell

models. Interestingly, when the equations mimicking the heterozygous state of the patients were introduced into the ventricular cell model, minor changes in AP morphology were observed (Supplemental Figure 6). Conversely, when the equations mimicking the heterozygous state were introduced in the Purkinje cell model, the effect was drastic: AP could not be induced (not shown). AP could be generated only if the shift in the activation curve was reduced (4 instead of 6 mV), in order to limit the Na^+ current increase (Supplemental Figure 6). But AP morphology was still highly affected. This disappeared at higher pacing rates, consistent with PVCs disappearing during exercise (Supplemental Figure 6).

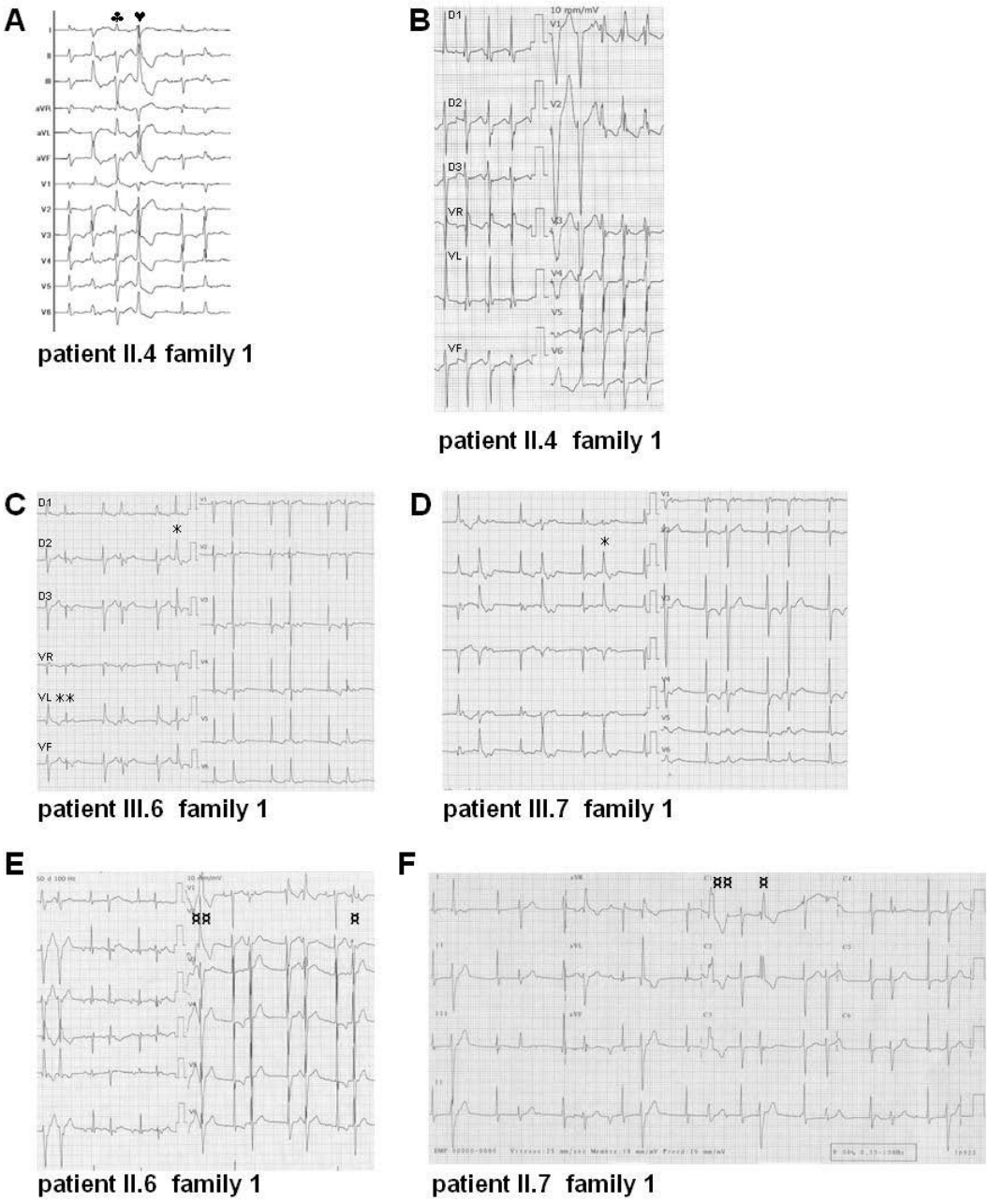

Supplemental Figure 1. Representative ECGs of family 1. Some patients (**A**) had PVC with RBBB patterns and alternant extreme variations in the axis from right (♣) to left (♥), from beat to beat. Recurrent monomorphic non-sustained ventricular tachyarrhythmia (NSVT) (**B**), and slightly polymorphic NSVT were also observed. In some patients, PVCs were relatively narrow QRS complexes (**C-D**), very similar to either sinus or junctional complexes with slight variations in the left axis from +60° (*) to -30° (**). In some patients (**E-F**), PVCs had RBBB patterns with various widths from relatively narrow (¤) to wide QRS complexes (¤¤).

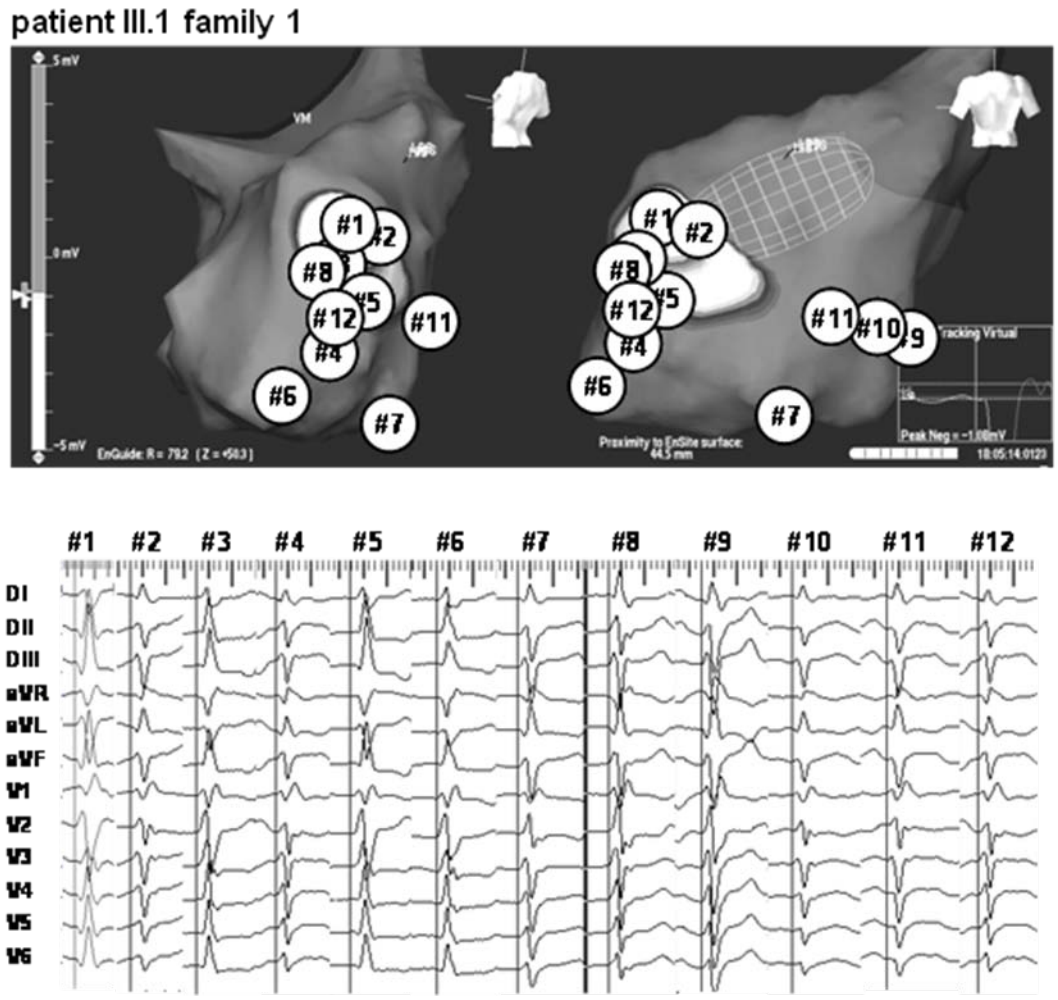

Supplemental Figure 2. Endocardial electroanatomic mapping of the left ventricle. Activation mapping of 12 different PVCs in patient III.1 (family 1). A Multi-array balloon (NavX system) helped us to pinpoint the precise location of ectopic foci along the anterior and posterior regions of the left ventricle corresponding to the extension of the left anterior and posterior fascicles.

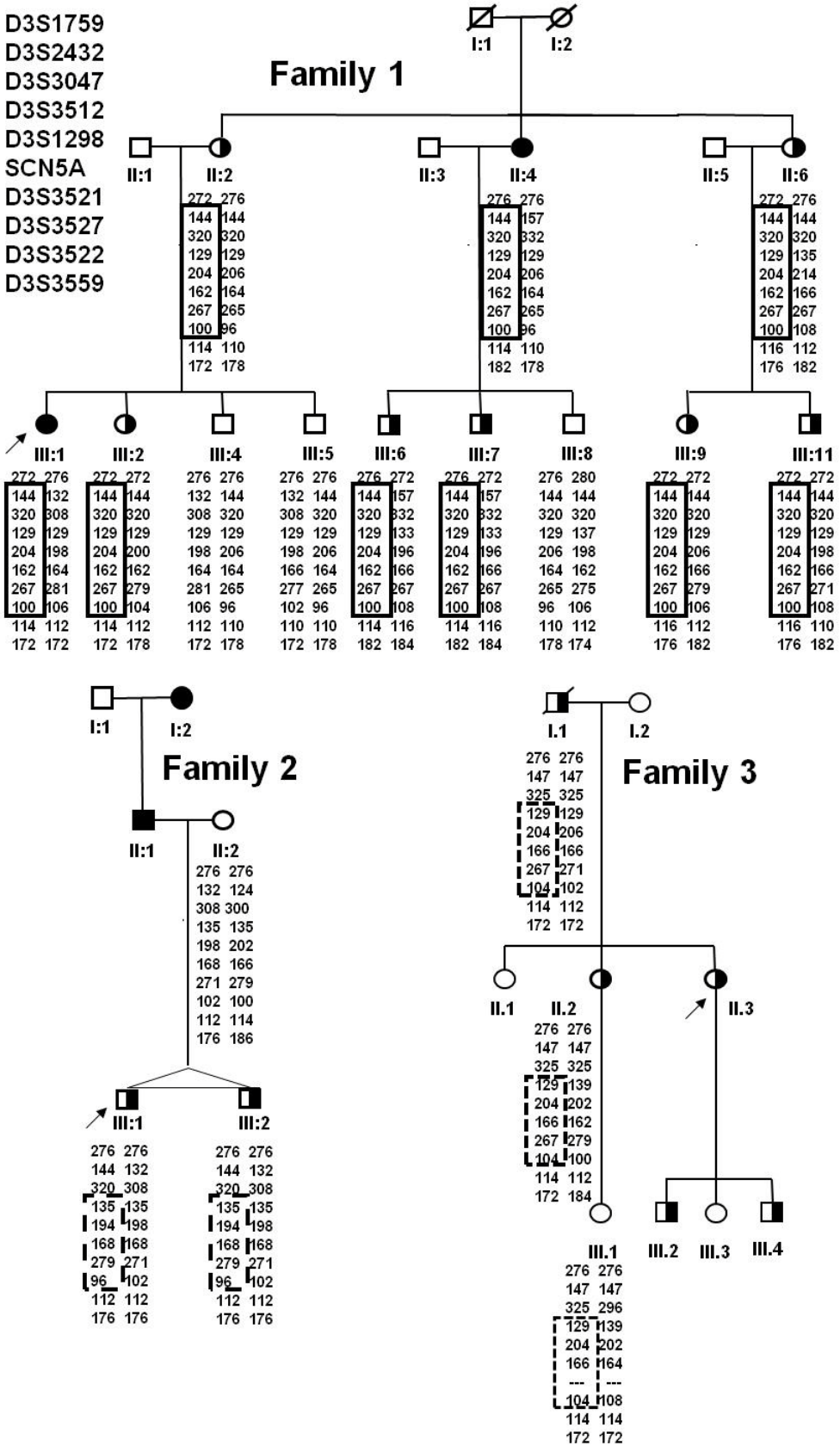

Supplemental Figure 3. Haplotype analysis of chromosome 3 in selected members for families 1, 2 and 3. Females are represented by circles and males are

represented by squares. Members affected with arrhythmia are indicated with a half-filled symbol. Members affected with arrhythmia and dilated cardiomyopathy (DCM) are indicated in black. Ten microsatellite markers (D3S1759, D3S2432, D3S3047, D3S3512, D3S1298, intragenic *SCN5A* marker, D3S3521, D3S3527, D3S3522 and D3S3559) spanning the region of chromosome 3 where the *SCN5A* gene lies, were analyzed. The disease-associated haplotype is indicated by a black frame. The disease haplotype in family 2 differed from that in family 1, showing that the R222Q mutation has arisen independently in these two families. Common alleles of two microsatellites are shared by families 1 and 3 implying a possible most recent common ancestor at least 28 generations earlier.

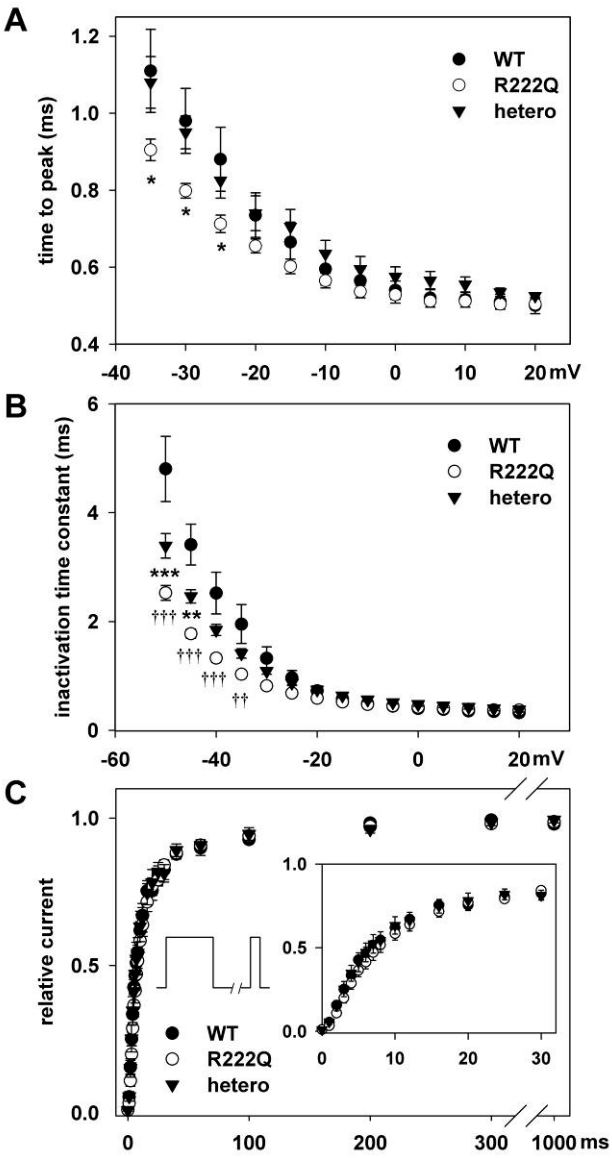

Supplemental Figure 4. Experimental effects of R222Q mutation on Nav1.5 channel in COS-7 cells. (**A**) Na^+ current time-to-peak values were used to evaluate the activation kinetics. Same transfection and voltage protocol as in Figure 4A. Tukey test: *, p<0.05 *vs* WT. (**B**) Accelerated inactivation in the presence of the R222Q mutation. Inactivation time constants were measured by fitting the inactivation phase of the Na^+ current to a single exponential equation. Tukey test: Heterozygous *vs.* WT, **: p<0.01, ***: p <0.001; R222Q *vs* WT, †: p<0.05, †††: p<0.001. (**C**) Recovery from inactivation was measured using a twin-pulse protocol (left inset: holding potential: –100 mV, 100-ms depolarization to -20 mV, back to -100 mV for 0 to 1000-ms delay before test pulse to -20 mV, frequency:0.1 Hz). Right inset: same as main graph for short delays.

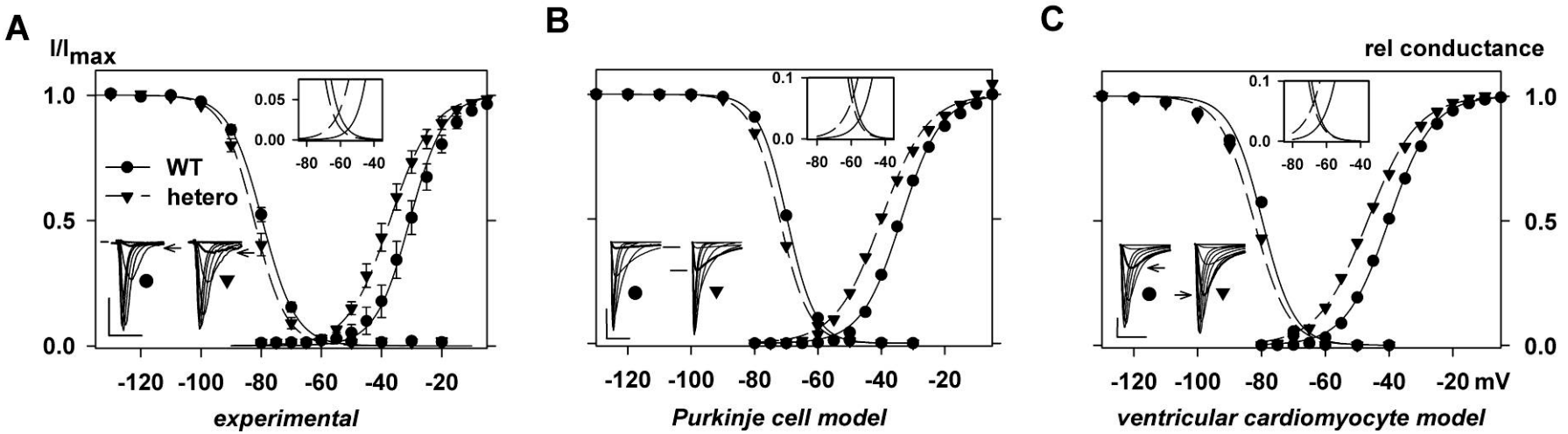

Supplemental Figure 5. (**A**) Superimposed activation and inactivation curves of WT (circles, solid line) and heterozygous (triangles, dashed line) channels obtained experimentally. Bottom inset: superimposed Na^+ current recordings using the same voltage protocol as in figure 4. Scale bars: 2 ms, 1000 pA. Top inset: increase of the predicted voltage window current in the presence of the mutation. (**B**) and (**C**) Simulated curves of WT (circles, solid line) and heterozygous (triangles, dashed line) channels; activation and inactivation in Purkinje cell (B) and (C) ventricular cardiomyocyte models. Bottom insets, simulated Na^+ currents as in A. Scale bars: 1 ms, 100 pA (B) and 5 ms, 100 pA (C). Top insets, as in A.

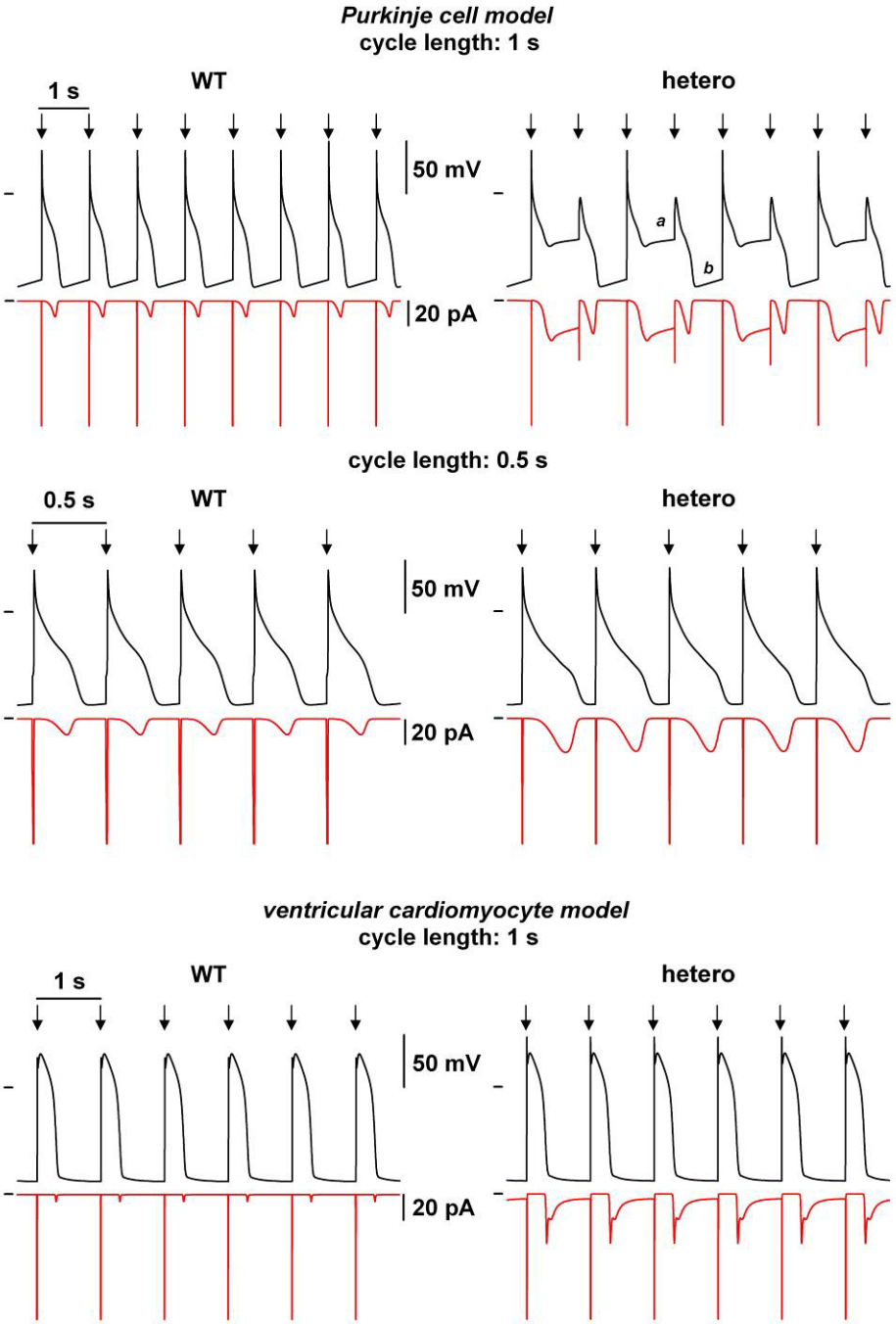

Supplemental Figure 6. Effects of the R222Q mutation on Purkinje (top) and ventricular (bottom) cell action potentials (APs) and Na^+ current obtained in the single-cell model. Simulated AP (black) and late Na^+ current (red) in WT (left) and heterozygous (right) conditions at the indicated cycle lengths. Arrows: external stimulus.

Supplemental movies

Simulation of the AP propagation from a Purkinje fiber to ventricular tissue (dimensions and stimulation shown in Figure 4), in WT (a) and heterozygous (b) conditions at cycle length of 1 s (A) and 0.5 s (B).

Supplemental Table 1: Effects of R222Q mutation on Nav1.5 biophysical parameters.

	current density	activation		inactivation		recovery from inactivation	window current		
	peak at –20 mV (pA/pF)	$V_{1/2}$ (mV)	k (mV)	$V_{1/2}$ (mV)	k (mV)	$t_{1/2}$ (ms)	g_{max} (pS/pF)	E_{max} (mV)	AUC (a.u.)
WT	–205.8±29.3 (36)	–30.6±2.1 (9)	5.7±0.3 (9)	–79.6±0.7 (10)	5.6±0.2 (10)	7.6±0.6 (6)	15.9±2.6 (13)	-42.8±0.5 (12)	29.9±3.9 (13)
heterozygous	–196.5±17.6 (48)	–37.2±1.6* (9)	7.1±0.3** (9)	–82.2±1* (9)	5.3±0.1 (9)	7.9±1.1 (8)	-	-	-
R222Q	–250.4±24.8 (44)	–42.3±1.0*** (11)	6.5±0.4 (11)	–84.6±0.7*** (8)	4.8±0.2** (8)	8.8±0.9 (8)	19.1±2.0 (14)	-58.6±1.1*** (14)	55.2±7.6** (14)

(n): number of cells; *: p<0.05; **: p<0.01; ***: p<0.001 *vs.* WT; $V_{1/2}$ and k; voltage for half-activation or -inactivation of the Na^+ current and slope; $t_{1/2}$: time to reach 50% recovery of the Na^+ current; g_{max}: maximal TTX-sensitive conductance recorded during a depolarizing-voltage ramp as in Supplemental Figure 4; E_{max}: potential at which the maximum conductance was measured. AUC: area under curve calculated on current density/membrane potential relationship; a.u.: arbitrary unit.

Supplemental Table 2: Effects of quinidine on WT and R222Q Nav1.5 currents.

		current density	window current
		peak at –20 mV (pA/pF)	**I_{max} (pA/pF)**
WT	**control**	–136.0±28.5 (12)	–1.87±0.42 (7)
	30 µM quinidine	–76.7±15.2***	–0.74±0.16*
R222Q	**control**	–123.3±20.1 (10)	–2.54±0.41 (6)
	30 µM quinidine	–63.9±10.5***	–1.17±0.12**

(n): number of cells; paired t-test: *: p<0.05; **: p<0.01; ***: p<0.001 *vs.* control; window current: TTX-sensitive (30 µM) current elicited by a depolarizing-voltage ramp; I_{max}: current density measured when the TTX-sensitive conductance is maximal (*i.e.* at -43 mV and -59 mV for WT and R222Q, respectively).

SUPPLEMENTAL REFERENCES

1 Bienengraeber M, Olson TM, Selivanov VA, Kathmann EC, O'Cochlain F, Gao F, Karger AB, Ballew JD, Hodgson DM, Zingman LV, Pang YP, Alekseev AE, Terzic A. ABCC9 mutations identified in human dilated cardiomyopathy disrupt catalytic KATP channel gating. Nat Genet. 2004;36:382-387.

2 Genin E, Tullio-Pelet A, Begeot F et al. Estimating the age of rare disease mutations: the example of Triple-A syndrome. J Med Genet 2004;41:445-449.

3 Brinkmann B, Klintschar M, Neuhuber F et al. Mutation rate in human microsatellites: influence of the structure and length of the tandem repeat. Am J Hum Genet 1998;62:1408-1415.

4 Kyndt F, Probst V, Potet F et al. Novel SCN5A mutation leading either to isolated cardiac conduction defect or Brugada syndrome in a large French family. Circulation 2001;104:3081-3086.

5 Loussouarn G, Park KH, Bellocq C et al. Phosphatidylinositol-4,5-bisphosphate, PIP2, controls KCNQ1/KCNE1 voltage-gated potassium channels: a functional homology between voltage-gated and inward rectifier K+ channels. EMBO J 2003;22:5412-5421.

6 DiFrancesco D, Noble D. A model of cardiac electrical activity incorporating ionic pumps and concentration changes. Philos Trans R Soc Lond B Biol Sci 1985;307:353-398.

7 Iyer V, Mazhari R, Winslow RL. A computational model of the human left-ventricular epicardial myocyte. Biophys J 2004;87:1507-1525.

8 Keener J, Sneyd J. Mathematical Physiology , 2nd edition. Springer, 2001.

9 Aslanidi OV, Stewart P, Boyett MR et al. Optimal velocity and safety of discontinuous conduction through the heterogeneous Purkinje-ventricular junction. Biophys J 2009;97:20-39.

10 Roden DM, Bennett PB, Snyders DJ et al. Quinidine delays IK activation in guinea pig ventricular myocytes. Circ Res 1988;62:1055-1058.

11 Sanchez-Chapula JA, Ferrer T, Navarro-Polanco RA et al. Voltage-dependent profile of human ether-a-go-go-related gene channel block is influenced by a

single residue in the S6 transmembrane domain. Mol Pharmacol 2003;63:1051-1058.

12 Wu L, Guo D, Li H et al. Role of late sodium current in modulating the proarrhythmic and antiarrhythmic effects of quinidine. Heart Rhythm 2008;5:1726-1734.

13 Wang Z, Fermini B, Nattel S. Effects of flecainide, quinidine, and 4-aminopyridine on transient outward and ultrarapid delayed rectifier currents in human atrial myocytes. J Pharmacol Exp Ther 1995;272:184-196.